Initial Suitability Evaluation of Steam-Reformed Low Activity Waste for Direct Land Disposal

B. P. McGrail
H. T. Schaef
P. F. Martin
D. H. Bacon
E. A. Rodriguez
D. E. McCready
A. N. Primak
R. D. Orr

January 2003

**WTP
Project
Report**

Battelle, Pacific Northwest Division
Richland, Washington 99352

LEGAL NOTICE

Initial Suitability Evaluation of Steam-Reformed Low Activity Waste for Direct Land Disposal

B. P. McGrail
H. T. Schaef
P. F. Martin
D. H. Bacon
E. A. Rodriguez
D. E. McCready
A. N. Primak
R. D. Orr

January 2003

Test Specification: 24590-LAW-TSP-02-007, Rev. 0
Test Plan: 44325-C2002-01, Rev. 0
Test Exceptions: None
Test Scoping Statements: FBSR-1

Prepared for Bechtel National, Inc
under Contract 24590-101-TSA-W000-00004 Task 10

Completeness of Testing

This report describes the results of work and testing specified by Test Specification 24590-LAW-TSP-RT-02-007, Rev 0 and Test Plan 44325-C2002-01, Rev. 0. The work and any associated testing followed the quality assurance requirements outlined in the Test Specification/Plan. The descriptions provided in this test report are an accurate account of both the conduct of the work and the data collected. Test plan results are reported. Also reported are any unusual or anomalous occurrences that are different from expected results. The test results and this report have been reviewed and verified.

Approved

_____   _____
B. Peter McGrail, PNWD Project Manager   Date

SUMMARY

A single sample of fluidized bed steam reformer (FBSR) product was subjected to detailed characterization and laboratory testing to determine whether the product would be an acceptable alternative to glass for immobilizing low-activity waste at Hanford. Because of funding and time limitations, insufficient testing was performed to fully assess the long-term performance of the product. However, the laboratory testing did provide a data set suitable for direct comparison with typical low-activity waste glasses tested under identical conditions. Single-pass flow-through tests (SPFT) were conducted in pH buffered solutions (pH 7 to 11) at 90°C to provide upper bounds on contaminant release rates. The results showed very little pH dependence for Re release, a non-radioactive element incorporated in the FBSR product as a chemical analog for ^{99}Tc. Normalized release rates ($g\ m^{-2}\ d^{-1}$) were found to be 100X slower than typical for ILAW glasses. However, because of the higher surface area of the FBSR product (based on BET gas adsorption measurements), as compared to glass per unit volume, total release rate from the FBSR product was estimated to be approximately 20 times higher than glass, again at 90°C. Use of the BET surface area for the FBSR product is the most conservative approach as it represents the upper limit on the possible exposed surface area of the product. The true reactive surface area could be 10X or more less than the BET surface area, so the actual difference in release rate probably ranges between 2 to 20 times higher than ILAW glass. Additional work will be required to better define the true reactive surface area of the FBSR product versus the geometric surface area used for normalization of the elemental releases from glass. Furthermore, temperature dependence of the release rate for the FBSR product was not determined so the relative release rate (irrespective of surface area assumptions) at the disposal system temperature of 15°C could not be evaluated.

The SPFT test is completely water saturated and typically run at quite high flow rate. Consequently, the test is not intended and certainly does not represent a typical vadose zone environment at Hanford. The pressurized unsaturated flow (PUF) test method was used to evaluate the performance of the FBSR product under conditions that more closely approximate the vadose zone. Problems were encountered early in the PUF tests with precipitation of lead sulfide particles on the porous plate mounted in the bottom of the PUF column, which is used to facilitate unsaturated flow during the test. In one test, the porous plate was removed and gravity drainage was used alone to establish unsaturated flow conditions. In the other test, the column was flushed with deionized water to remove fine particles; the test was then restarted. Despite these difficulties, reasonably good test data was obtained and Re release rates were computed from the measured effluent composition. These data were converted to fractional release rate values and compared with PUF test data obtained on a reference ILAW glass, LAWA44. Use of the fractional reslease rate normalizes out the differences in relative surface area and so provides the best measure for comparison of the relative durability between the two waste forms. Results from the PUF tests showed equivalent fractional release rates for the FBSR product and LAWA44 glass within experimental error. The combination of the SPFT and PUF test data suggest that a FBSR product would likely be an acceptable alternative ILAW form. We recommend additional testing to reach a scientifically defensible conclusion regarding FBSR product performance under disposal system conditions.

Page left intentionally blank.

CONTENTS

FIGURES

TABLES

Page left intentionally blank.

1.0   INTRODUCTION

In December 2001, Bechtel National Inc. (BNI) and Washington Group International Inc. contracted with Studsvik Inc. (Erwin, Tennessee) to perform a demonstration test of its fluidized bed steam reformer (FBSR) technology for denitration and stabilization of simulated pretreated low-activity waste (LAW). Briefly, the THOR™ FBSR process operates by introducing high sodium nitrate content tank wastes into a moderate temperature (650-800°C) fluidized bed vessel operating under vacuum. The tank waste is reacted with carbon and iron-based reductants to convert nitrates and nitrites directly to nitrogen gas. Radionuclides, alkali metals, sulfate, chloride, fluoride, and non-volatile heavy metals in the waste stream are reacted with clay (kaolinite) or other inorganic materials to produce a polycrystalline mineral product. Additional details on the process can be found in the report by Jantzen (2002) or at the THOR Treatment Technologies, LLC website (www.thortt.com).

The FBSR product used in the testing discussed in this report was manufactured in a 6-inch diameter, fluidized bed pilot plant at Hazen Research (Golden, Colorado). Processing was performed for relatively short periods so that a number of variations to the THOR™ steam reformer technology could be demonstrated. The variations included different additives to the feed that produced a minimum of two different sodium aluminosilicate phases (nepheline and nosean) and sometimes a second polymorph of the nepheline in the solid product. Operating parameters were also adjusted during the operation to determine these effects on the product and on pilot operation. Product produced using the steam reformer technology tested passed (JANTZEN, 2002) the Toxicity Characteristic Leaching Procedure (TCLP) and is being evaluated as a candidate waste form suitable for direct burial at the Hanford site. However, not all the LAW RCRA constituents were in the simulant so additional evaluation of a qualified simulant is still needed.

In July of 2002, BNI requested that Battelle conduct a testing program to provide data that would support a preliminary assessment of the performance of a FBSR product under simulated shallow land disposal conditions at Hanford. The work to be conducted was delineated in a Test Specification prepared by BNI (ABEL, 2002). Battelle conducted two different tests, the single-pass flow-through (SPFT) and pressurized unsaturated flow (PUF) test. These tests form part of the recommended strategy for evaluating long-term waste form performance for the LAW disposal system (MCGRAIL et al., 2000a) and have been used extensively to evaluate various LAW glass formulations (MCGRAIL et al., 2001a; MCGRAIL et al., 2002). The results and conclusions from this testing program are summarized in this report. In the next Section, we first discuss results from characterization of the specific FBSR product used in these tests. Characterization of the test material is, of course, critical to the analyses and interpretation of the test data presented in this report.

Quality assurance requirements for this work were provided by BNI in Test Specification (ABEL, 2002), Initial Suitability Evaluation of Steam-Reformed LAW for Direct Land Disposal. The work outlined in this report is a scoping evaluation of the corrosion behavior of steam reformer material produced during an initial field experiment. Therefore, the laboratory tests were performed in accordance with the basic quality assurance requirements stated within 10 CFR 830 (Subpart A), NQA-1 (1989), and NQA-2a (1990) Part 2.7, graded according to the nature, importance and level of complexity of the scoping effort. The *Quality Assurance Requirements and Description* (DOE/RW-00333P), the principal quality assurance document for the Civilian Ra-

dioactive Waste Management Program does not apply to activities conducted as part of this work. This work is not in support of environmental/regulatory testing and therefore the QAPjP, 24590-QA-0001, does not apply. Applicable elements/procedures of the Waste Treatment Plant Support Project Quality Assurance Requirements and Description Manual (WTPSP) were implemented in this work.

2.0   PRODUCT CHARACTERIZATION

A jar of the FBSR product labeled SCT02-098 was received from BNI. Characterization of the product was conducted following well-established procedures. The methods used and results are discussed in the following sections.

2.1   BULK COMPOSITION ANALYSIS

2.1.1   Fusion Procedure

FBSR product samples analyzed by inductively coupled plasma-optical emission spectroscopy (ICP-OES), inductively coupled plasma-mass spectrometry (ICP-MS), and Ion Chromatography (IC) were fused by two different methods, which used either Na_2O_2 or $LiBO_2$. To determine whether crushing and sieving to specific mesh sizes used in testing introduced artifacts in the sample composition, duplicate analyses were conducted on product sieved to one of two sizes, 2.0 to 0.85 mm (-10+20 mesh) or 150 to 75 µm (-100+200 mesh). The -10+20 mesh sample was obtained directly from the original product sample without further preparation beyond sieving. The -100+200 mesh sample was obtained from product that had been crushed by hand with an agate mortar and pestle. Approximately 0.05 g to 0.1 g of the sieved product was mixed with reagent grade chemical (Na_2O_2 or $LiBO_2$) in a Pt crucible. The crucibles were covered and transferred to a muffle furnace (605°C Na_2O_2, and 1000°C $LiBO_2$). After 20 minutes of heating at the required temperature, the crucibles were removed and cooled. Concentrated HNO_3 acid was added to each crucible and gently heated over a hot plate until the fused samples dissolved. The fusions were diluted up to a total volume of 100-mL with deionized water and submitted for analysis. The acidification step was omitted for the fusion sample submitted for IC analyses.

2.1.2   X-Ray Fluorescence Procedure

Insoluble or difficult to dissolve compounds can sometimes give erroneous composition results in chemical fusions. Consequently, a complementary, non-wet chemical method is used in our laboratory as an independent check of chemical fusion data. The same FBSR product samples used for the chemical fusions were analyzed by x-ray fluorescence (XRF) spectroscopy. Samples were first homogenized in a Coors high-density alumina mortar and pestle. Six hundred milligrams of the homogenized sample was removed and ground a second time to approximately 300 mesh. For energy dispersive x-ray fluorescence, a sample was placed between two sheets of stretched parafilm and loaded into a Kevex 0810A x-ray fluorescence unit. For wavelength dispersive x-ray fluorescence, the ground sample was pressed into a 3.2 cm diameter pellet and placed in a Siemens Spectra 3000 instrument equipped with a flow detector for analysis of soft radiation from low Z elements and a scintillation detector for analysis of higher energy radiation from high Z elements.

2.1.3   Results

Results from the chemical analysis of the FBSR product are shown in Table 1. In general, our results agree quite well with the previous analysis of Jantzen (2002), which is provided in Table 1 for reference. However, analysis of the FBSR product according to size fraction shows significant compositional differences with respect to Al, Fe, Na, and Si content. Visual observation during sample preparation indicated particles with various levels of hardness in the product,

Table 1. Bulk Compositional Analysis (Mass %) of FBSR Product SCT02-098

Oxide	Jantzen	Fusions		Method	XRF		
		-10+20	-100+200		-10 +20	-100 +200	Fines
Ag_2O	nr	0.0029	0.0029	MS	BLQ	BLQ	BLQ
Al_2O_3	31.740[a]	39.246	32.133	OES	32.473	29.915	24.992
CaO	0.7332	0.8512	0.7819	OES	0.6651	0.5531	0.7430
Cl	nr	0.2159	0.2159	IC	0.0707	0.0839	0.0994
Cr_2O_3	0.0716	0.0344	0.0461	MS	0.0451	0.0603	0.0395
Cs_2O	0.0029	0.0009	0.0012	MS	0.0323	0.0360	0.0297
F	nr	0.0056	0.0056	IC	BLQ	BLQ	BLQ
Fe_2O_3	5.4471	7.2725	5.0056	OES	7.1382	4.7855	1.9740
FeO	0.8749	nd	nd		nd	nd	nd
K_2O	0.6975	0.7100	0.8400	OES	0.6866	0.7680	0.6746
Li_2O	nr	0.2445	0.2187	MS	BLQ	BLQ	BLQ
MgO	nr	0.1366	0.1326	OES	0.0541	0.0528	0.0480
MnO	nr	0.0743	0.0254	OES	0.0735	0.0263	0.0262
MoO_2	nr	0.0053	0.0050	OES	0.0247	0.0215	0.0379
Na_2O	19.815	16.870	21.227	OES	17.052	18.821	29.660
NiO	0.0814	0.0398	0.0571	MS	0.0440	0.0675	0.0477
P_2O_5	0.2176	0.2499	0.2057	OES	0.2443	0.1850	0.2257
PbO	0.0175	0.0182	0.0182	OES+MS	0.0247	0.0272	0.0647
ReO_2	0.0005	0.0005	0.0007	MS	BLQ	BLQ	BLQ
SiO_2	34.870	29.336	37.526	OES	37.931	42.055	39.039
SO_3	0.9310[b]	0.8107	0.9297	OES	0.6220	0.6819	0.6967
TiO_2	nr	1.6228	1.2617	OES	1.8307	1.4853	1.2626
V_2O_5	nr	0.0685	0.0311	MS	0.0318	0.0140	0.0157
ZnO	nr	0.0184	0.0159	OES+MS	0.0080	0.0086	0.0068
ZrO_2	nr	0.1157	0.0300	OES+MS	0.1250	0.0293	0.0283

BLQ = Below Limit of Quantification; nr = not reported; nd = not determined
[a]Five significant figures are shown to accurately capture the low concentration of ReO_2 in the sample. Mass percents of oxides with concentrations above 0.001% should not be considered accurate to five significant figures.
[b]Converted from SO_4 value reported by Jantzen

some later identified as magnetite, that were more resistant to crushing than the bulk of the material. Thus, these particles tended to be separated out at smaller size fraction, which is reflected in the chemical analysis. Consequently, caution is required with respect to reporting a bulk composition for the FBSR product as it will be dependent on the sample preparation method and particle size selected for analysis. The reader should also note that rhenium was added to the simulated LAW stream used to make the FBSR product as a non-radioactive chemical analog for ^{99}Tc, which is the most important dose contributor as determined from the 2001 ILAW performance assessment (MANN et al., 2001).

2.2   X-RAY DIFFRACTION ANALYSIS

X-ray diffraction measurements were also performed with the -10+20 and -100+200 mesh size fractions used in PUF and SPFT testing, respectively. In the -10+20 size fraction, the identified crystalline phases are the hexagonal form of nepheline ($NaAlSiO_4$, PDF #35-0424), nosean [$Na_8(AlSiO_4)_6SO_4$, PDF #17-0538)], mullite ($Al_6Si_2O_{13}$, PDF #15-0776), hematite (Fe_2O_3, PDF #33-0664), magnetite (Fe_3O_4, PDF #19-0629) and corundum (Al_2O_3, PDF #71-1123). With the exception of mullite, these are the same phases identified by Jantzen (2002). However, mullite and corundum were not detected in our -100+200 mesh size fraction. In addition to bulk composition, size fractionation also has an important effect on the mineralogical makeup of the FBSR product.

2.3   RAMAN SPECTROSCOPIC ANALYSIS

A Raman spectrum was recorded for the FBSR product and for a natural nepheline mineral sample obtained from Bancroft, Ontario, Canada (Ward's Natural Science, Inc. #48E5580). The Raman scattered light was collected at room temperature in 180° mode with a fiber optic probe. Scattered laser light is passed through a holographic notch filter with an optical density of 4 but 80% transmissivity for Raman scattered light. The probe is coupled to a Holospec (Kaiser Optical Systems) spectrograph. The spectrograph features fast f/1.8 optics, HoloPlex™ transmission grating, and back-illuminated CCD detector. Incident light was provided by a 532 nm diode-pumped ND:YAG laser delivering approximately 150 mW at the sample surface. The fiber optic probehead was mounted on a motorized, digital X-Y translation table. Movement of the probehead was controlled through a custom computer software program that moved the probehead in a circular pattern while the camera shutter was open. This allowed us to substantially increase the laser coverage across the material instead of focusing on a single spot with a beam diameter of about 0.7 mm. Consequently, the collected spectrum is more representative of the overall material.
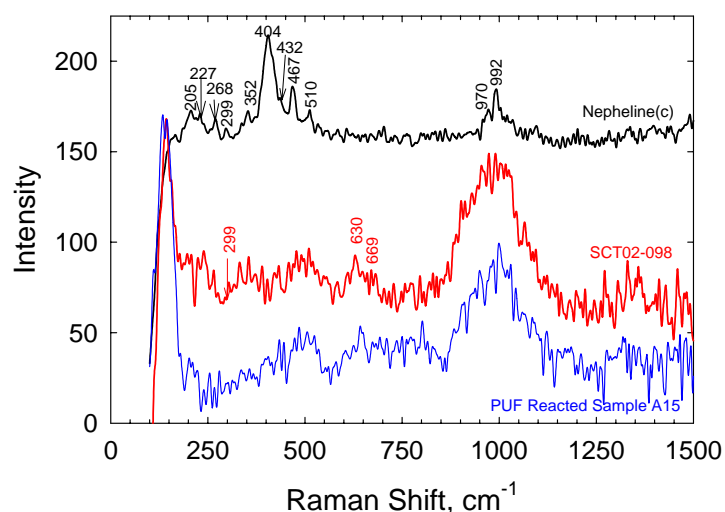
Figure 1. Raman Spectra of FBSR Product and Crystalline Nepheline

A comparison of the Raman spectra from the nepheline sample and the FBSR product are shown in Figure 1. Although the Raman spectrum for the FBSR product is nepheline-like, the spectrum actually more closely resembles glassy nepheline (MATSON et al., 1986) than the crystalline form. The dominant feature of the spectrum is a broad band between 900 and 1100 cm^{-1}. Vibrational modes in this region are assigned to antisymmetric stretching mode vibrations for SiO_4 and AlO_4 tetrahedra. Mode splitting occurs from the lowering of site symmetry from pure tetrahedral because of the differing T-O bond characteristics associated with adjacent SiO_4 versus AlO_4 tetrahedra. Line broadening also likely occurs because of substitution of Ti and other

metals into the nepheline structure. The Raman spectra are also consistent with a detailed analysis of the XRD pattern, which shows slightly shifted d-spacings from the PDF reference spectra for nepheline.

3.0   SINGLE-PASS FLOW-THROUGH TESTING

To predict the long-term fate of glasses in the subsurface over the period of regulatory concern, a mathematical model that describes glass reactivity is needed. The model used for glass in the 2001 ILAW performance assessment (MANN et al., 2001) is based upon the Transition State Theory of chemical kinetics in which the overall reaction rate is governed by the slowest elementary reaction. A general equation describing the rate of reaction as a function of solid (glass or mineral) composition, pH, temperature, saturation state of the system, and the activities of rate-enhancing or -inhibiting entities is (Aagaard and Helgeson, 1982):

$$ r \;=\; \bar{k} a_{\mathrm{H^+}}^{-\eta} \exp\!\left(\frac{-E_a}{\mathrm{RT}}\right) \left[1 - \left(\frac{Q}{K_g}\right)^{\sigma} \right] \prod_j a_j \tag{1} $$

where: r = dissolution rate, g m^{-2} d^{-1}
$\bar{k}$ = intrinsic rate constant, g m^{-2} d^{-1}
$a_{\mathrm{H^+}}$ = hydrogen ion activity
a_j = activity of the jth aqueous species
E_a = activation energy, kJ/mol
R   = gas constant, kJ/mol·K
T   = temperature, K
Q = ion activity product
K_g = pseudoequilibrium constant
η = pH power law coefficient
σ = Temkin coefficient.

By manipulating one experimental condition, such as temperature, flow-rate, pH, and the concentration of additives, while keeping the others constant, the parameters within Equation (1) can be isolated and quantified (MCGRAIL et al., 1997a). A convenient experimental technique to implement these conditions is the single-pass flow-through (SPFT) method (KNAUSS et al., 1990; MCGRAIL et al., 1997a).[a]

Use of the SPFT method for parameterization of Equation (1) is only strictly valid for a homogeneous, single phase material. Because the FBSR product is polyphase, the SPFT method will provide a convoluted signal that represents the combined release from each of the phases present. Separation of the contributions from the individual phases would require information on the dissolution kinetics of each phase in the product. Some dissolution kinetics data exists for phase pure crystalline nepheline (TOLE et al., 1986; HAMILTON et al., 2001). However, we have not been able to locate any direct measurements of the dissolution kinetics of nosean and only sparse data is available for analog phases such as sodalite [Na$_8$(AlSiO$_4$)$_6$(Cl)$_2$] (MORSS et al., 2000; JEONG et al., 2002). Longer-term dissolution kinetics may also be controlled by the slowest reacting primary phase. Nevertheless, the SPFT test can provide bounding, overall release rate data from the product under dilute solution conditions. These data can also be compared with the extensive SPFT database that has been collected on ILAW glasses in our laboratory.

---

[a]A draft procedure for the SPFT method is currently under review by the ASTM.

3.1 EXPERIMENTAL METHODS

The dissolution kinetics of the FBSR product was quantified through the use of single-pass flow-through (SPFT) tests. The SPFT test is an open system experiment where a solution at a known flow rate and constant temperature flows through a reaction cell that contains the sample. The configuration precludes recirculation of the effluent and so makes a "single-pass" through the reaction cell. Many different SPFT apparatuses have been developed, but these can all be classified as three basic types: 1) well-mixed batch, 2) packed bed, and 3) fluidized bed. The well-mixed batch type of apparatus was used for all test data reported here. The usefulness of SPFT experiments stems from the system reaching a steady-state condition between the test material and the aqueous solution. Steady-state conditions ensure the system is maintained at constant chemical affinity and the effluent is at a constant value of pH. These conditions are necessary to isolate chemical reactions that are normally affected by several parameters.

3.1.1 Materials Preparation

Crushing the FBSR product in an agate mortar and pestle produced the sample used in this study. The crushed material was then sieved to separate the <100, >200 mesh (150 to 75 μm diameter) size fraction. The powdered sample was then sonicated in absolute ethanol three times to remove any adhering particles outside the desired size fraction. We also subjected a few grams of the ethanol-cleaned sample to an additional sonication wash step in deionized water. This was done to test for removal of any water-soluble salt phases. After drying in a 90°C oven for several hours, the powder was kept in a dessicator until used in an experiment. The specific surface area of the sample was determined to be at 2.37 ±0.5 m^2/g by averaging three separate N_2 BET (BRUNAUER et al., 1938) measurements. One can also estimate the specific surface area based on the following geometric formula (MCGRAIL et al., 1997a):

$$s = \frac{3}{\rho r} \tag{2}$$

where, ρ is the sample density (g m^{-3}), and r is the average particle radius in meters. The density of the FBSR was measured with an Accupyc 1330 He pycnometer at 2.764 ±0.004 g/cm^3. Using this value in Equation (2), the calculated geometric surface area is 0.0193 m^2/g, which is 120 times less than the measured value via BET.

It must be recognized that in dissolution kinetics experiments, the proper handling of surface area is one if not the most problematic variable, and has been the subject of numerous studies (BRANTLEY and MELLOTT, 2000). A large degree of uncertainty is associated with measurements of bulk BET surface area, and the contribution of actual reactive surface area is not always known. With glasses, considerable evidence has been developed (MCGRAIL et al., 1997a) showing no break in dissolution rates when transitioning from monoliths to glass powders, assuming the geometric surface area for the glass powders is used to calculate dissolution rates. Glasses have no microporosity and surface artifacts introduced from grinding only affect dissolution rates at early times. In contrast, Anbeek et al. (1994) showed that dissolution rates of mesoporous feldspar and quartz grains varied as a function of grain size when using geometric surface area to calculate the rates. They attributed this observation to the contribution of micropores to the release rates. However, Brantley and Mellott (2000) point out that surface area measured by gas adsorption may not be appropriate for extrapolation of interfacial controlled dissolution of many

silicates if internal surfaces are present that are substantially less reactive than the external surfaces.

Scanning electron microscopy of FBSR grains (Figure 2) shows a highly irregular surface and considerable microporosity. This morphology is obviously inconsistent with a pure geometric representation of the particle surface as represented via Equation (2). Furthermore, we have no evidence to support arguments regarding lower reactivity of the mineral surfaces in the interior of the grains or in the mesopores. Consequently, we have elected to use the BET surface area for the calculation of dissolution rates from the SPFT analytical data (see below). The reader should be aware that use of the BET surface area is the most conservative approach as it represents the upper limit on the possible exposed surface area of the product. The true reactive surface area is probably less, and perhaps substantially less than the BET value but also probably significantly higher than the geometric value. Additional work will be required to better constrain the reactive surface area of the FBSR product.

Figure 2. SEM Micrograph of Typical FBSR Product Grain

Optical photographs also show the presence of small dark particles dispersed throughout the product, as illustrated in Figure 3. We were able to separate these dark particles by passing a magnet over the sample and XRD analyses confirmed that these particles are magnetite. As magnetite is used in the FBSR process, the presence of this mineral is not surprising.

3.1.2 Solutions

Figure 3. Optical Photograph of SCT02-098 Particle. Black particles are magnetite

Five different solutions were used to control the pH during the experiments and are listed in Table 2. Neutral to slightly basic solutions (pH = 7, 8, 9, and 10) were made by adding small amounts of the organic THAM (*tris hydroxymethyl aminomethane*) buffer to DIW and then adding minor concentrations of HNO_3 to bring the solution to the desired pH value. Alkaline solutions (pH = 11) were prepared by adding LiCl and LiOH to DIW. Table 2 also gives the change in pH with respect to the temperature of the experiment, as calculated with the EQ3NR geochemical code (Wolery, 1992). As one can see from Table 2, the *in-situ* pH of the experiment can change by as much as 1.5 pH units over the temperature interval of 23 to 90°C. All testing was conducted at 90°C. Aliquots of all input solutions used in this study were analyzed by ICP-OES and ICP-MS methods to determine the background concentration of elements of interest (Al, Si, Na, Re, etc.).

Table 2. Composition of Solutions Used in SPFT Experiments. TRIS = THAM-based buffer. Solution pH values above 23°C were calculated with EQ3NR Code V7.2b database.

Solution #	Composition	pH 23ºC	pH 40ºC	pH 70ºC	pH 90ºC
1	0.01 M TRIS + 0.0093 M HNO₃	7.13	6.53	5.87	5.50
2	0.01 M TRIS + 0.0059 M HNO₃	8.08	7.54	6.88	6.52
3	0.05 M TRIS + 0.0079 M HNO₃	8.97	8.44	7.78	7.42
4	0.05 M TRIS	9.65	9.38	8.87	8.52
5	0.01 M LiCl + 0.0107 LiOH	11.07	10.94	10.49	10.12

3.1.3 SPFT Apparatus

The salient features of the single pass flow-through (SPFT) apparatus used in this study have been described in detail elsewhere (MCGRAIL et al., 2001b). A syringe pump (Kloehn; model 50300) was used to transfer solution from a N_2 sparged reservoir bottle to a Teflon® PFA reactor. Up to four experiments per pump could be run using the same input solution. Transport of solution from the pumps was accommodated by 1/16th inch Teflon® PFA tubing. The oven was set to the temperature of interest and a digital thermocouple, accurate to ±2°C, was used to record temperature daily. An in-line reservoir situated in the oven before the reactor was also used because the typical flow-through rates were fast enough that solution may not have had time to equilibrate at the temperature of interest before entering the reactor. The reservoir vessel contains two ports, for inflow and outflow of solution. A Teflon® line connected the reservoir to the reactor, which housed the powdered sample. The reactors consist of two pieces that screw together with the upper half containing a port for ingress of solution and a second port for the egress of effluent solution. We used 0.5 ±0.004g of -100+200 mesh sample in each reactor; the powder lies at the bottom of the reactor in a thin layer. Therefore, the fluid is not pumped directly through the sample, as in other reactor designs. The advantage of this design is that bubbles that form in the fluid transfer lines do not become entrained in the sample, which could alter the exposed surface area. Effluent is collected continuously in collection bottles situated outside the oven.

Aliquots of effluent solution were routinely checked to ensure that pH control was maintained during the experiment. The remainder of the effluent solution was acidified by high purity nitric acid and analyzed for chemical composition by ICP-OES and ICP-MS methods. Three blank solutions were drawn before the FBSR sample was added to the reactor. The blank solutions were analyzed for background concentrations of elements of interest. The experiments were terminated after 23 days reaction time. At the lowest flow rate used (60 mL/d), over 34 reactor volumes of fluid were exchanged over this time period. Since it typically takes exchange of seven reactor volumes to achieve steady-state conditions (Westerterp et al., 1983; Fogler, 1986), the duration of the experiments is more than sufficient to eliminate any "dead volume" effects from the original starting fluid in the reactor.

3.2 DISSOLUTION RATE AND ERROR CALCULATIONS

Dissolution rates are calculated from the measured concentrations of elements in the effluent, normalized to the amount of the element present in the waste form sample using the following formula:

$$\text{Normalized dissolution rate (g m}^{-2}\text{d}^{-1}) = \frac{(C_i - \overline{C}_{i,b})q}{f_i S} \tag{3}$$

where C_i is the concentration of the element, i, in the effluent (g L^{-1}), $\overline{C}_{i,b}$ is the average background concentration of the element of interest (g L^{-1}), q is the flow-through rate (L d^{-1}), f_i is the mass fraction of the element in waste form (dimensionless), and S is the surface area of the sample (m^2). The values of f_i for the FBSR product were calculated from the chemical fusion data given in Table 1 for the -100+200 mesh size fraction. Flow-through rates were determined by gravimetric analysis of the fluid collected in each effluent collection vessel upon sampling. The background concentration of the element of interest is determined, as previously discussed, by analyses of the starting input solution and the three blank solutions. Typically, background concentrations of elements are below their respective limits of quantification (LQ). In cases where the analyte is below the detection threshold, the background concentration of the element is set at the value of the detection threshold.

Determining the experimental uncertainty of the dissolution rate takes into account uncertainties of each parameter in Equation (3). For uncorrelated random errors, the standard deviation of a function $f(x_1, x_2,...x_n)$ is given by:

$$\sigma_f = \sqrt{\sum_{i=1}^{n} \left(\frac{\partial f}{\partial x_i} \right)^2 \sigma_i^2} \tag{4}$$

where

σ_f = standard deviation of the function f.
x_i = parameter i
σ_i = standard deviation of parameter i.

In the case of dissolution of a solid, the function of interest is Equation (3). Substituting Equation (3) into Equation (4) results in:

$$\sigma_{r_i} = \sqrt{\left(\frac{q}{f_i S} \right)^2 (\sigma_{C_i}^2 + \sigma_{\overline{C}_{i,b}}^2) + \left(\frac{C_i - \overline{C}_{i,b}}{f_i S} \right)^2 \sigma_q^2 + \left(\frac{(C_i - \overline{C}_{i,b})q}{f_i^2 S} \right)^2 \sigma_{f_i}^2 + \left(\frac{(C_i - \overline{C}_{i,b})q}{f_i S^2} \right)^2 \sigma_S^2} \tag{5}$$

Equation (5) can also be expressed in terms of the relative error, $\hat{\sigma}_{r_i} = \sigma_{r_i} / r_i$, and is given by

$$\hat{\sigma}_{r_i} = \sqrt{\frac{\left(\hat{\sigma}_{C_i} C_i \right)^2 + \left(\hat{\sigma}_{\overline{C}_{i,b}} \overline{C}_{i,b} \right)^2}{\left(C_i - \overline{C}_{i,b} \right)^2} + \hat{\sigma}_q^2 + \hat{\sigma}_{f_i}^2 + \hat{\sigma}_S^2} \tag{6}$$

Typical relative errors determined from extensive previous testing for C_i, $\overline{C}_{i,b}$, q, f_i, and S are 10%, 10%, 5%, 3%, and 30%, respectively. Although the absolute error in f_i is likely to be significantly higher than 3%, this error is non-systematic and so does not contribute significantly to sample-to-sample uncertainty, which is the principal error of interest here. The conservative appraisal of errors assigned to the parameters in Equation (6) results in maximum uncertainties of approximately ±35% on the dissolution rate.

3.3   RESULTS

3.3.1   Temporal Release Behavior

Each SPFT experiment was run in duplicate. However, we will only show the results from one of the experiments as the data were essentially identical for each replicate test. Detailed results from each test are provided in Appendix A. Figure 4 shows the results for all five of the pH values tested. Immediately obvious from these data is a strong correlation between the release behavior of S and Re. Rhenium and sulfur release rates are usually the fastest, except at the
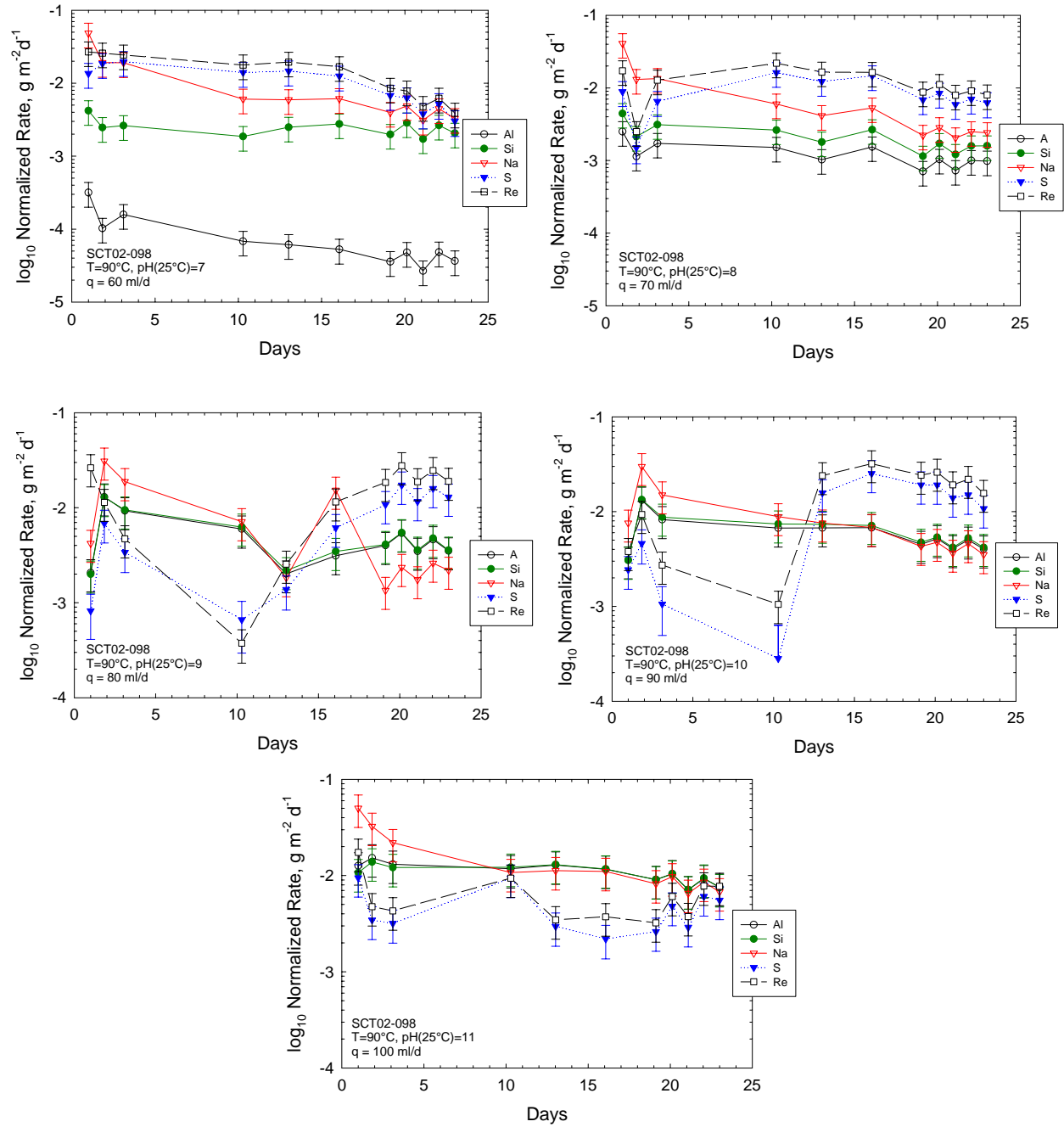
Figure 4. Normalized Release Rate as a Function of Time and pH in SPFT Experiments at 90°C

highest pH value we tested (pH 11). A possible interpretation of these results is that Re and S are incorporated in the same phase and so the release kinetics is being controlled by the dissolution behavior of this primary phase. Mattigod et al. (2002) have successfully synthesized and done the structural refinement for perrhenate sodalite. The sodalite group has the general formula $Na_8(AlSiO_4)_6(M)_2$. Sodalite has a cage-like structure and can accommodate a number of oxo-anions (M). Nosean is the sulfate form of sodalite (M = ½SO_4). Since perrhenate sodalite (M = ReO_4) has now been synthesized, it could be present in the FBSR product. However, the very small amount of Re in the product made it impossible to isolate and identify this phase, even if it is present in the product.

3.3.2 Deionized Water Washing Effects

The fraction of sample prepared with a deionized water wash step was tested for comparison with the sample washed in absolute ethanol only. The experiment, also run in duplicate, was conducted at pH 9 and flow rate of 80 ml/d. A comparison of the results in Figure 5 with those in Figure 4 shows no significant differences. There is still a strong correlation between the release rates of Re and S, which are the highest release rates measured at the pH value of 9. These data show no evidence of significant highly water-soluble salt phases present in the material.

3.3.3 Effect of Flow Rate

In addition to the pH dependent measurements, a second series of SPFT experiments was performed to examine the dependence of the measured dissolution rates as a function of flow rate. These experiments were performed in the same manner as the first series but flow rates were varied from a low of 20 mL/d to a maximum of 200 mL/d. The same buffer solution (pH 9) was used for each flow rate. Detailed results from these experiments are provided in Appendix A. In Figure 6, dissolution rates obtained by averaging the last three data points collected for each flow rate are plotted versus the imposed solution flow rate in the test. The results show the expected decline in release rate with decreasing flow rate for Na, Al, and Si, which are the principal components in the major mineral component, nepheline. The decrease in release rate is consistent with an expected decrease in the dissolution rate of nepheline as the solution concentrations increase at slower flow rates. Note that at about 140 mL/d flow rate and higher, release rates become independent of the flow rate and so indicate the true forward rate of reaction.
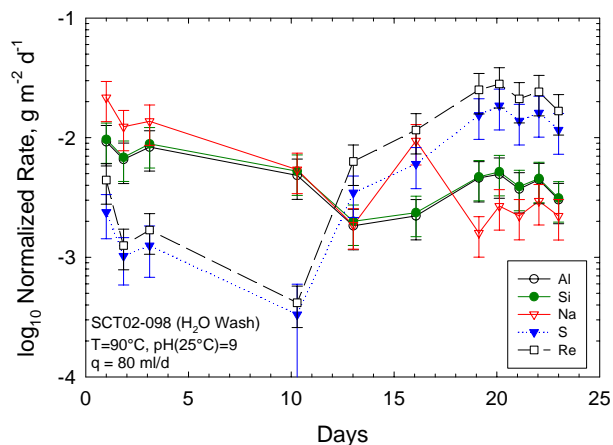
Figure 5. Normalized Release Rate as a Function of Time on Deionized Water Washed Material in SPFT Experiment at 90°C
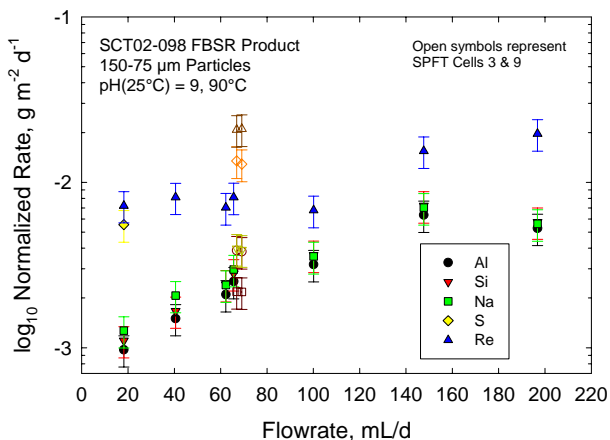
Figure 6. Normalized Release Rate as a Function of Solution Flow Rate in SPFT Experiments at pH(25°C) = 9, and 90°C

In contrast, Re release is observed to be essentially independent of flow rate over the range studied. If the Re is present principally in the nosean phase as was discussed previously, the data indicate that nosean is dissolving at what appears to be a forward rate of reaction over the entire flow rate range studied. This result is not unexpected as nosean should only be stable under alkaline pH conditions. Additional evidence supporting this hypothesis is discussed in the next section.

3.3.4 Effect of Solution pH

The steady-state release rates for the major components in the FBSR product, obtained by averaging the last three samplings shown in Figure 4, are plotted as a function of pH in Figure 7. The data for nosean (represented by S and Re) show a decline in the reaction rate at pH(90°C) > 8. This behavior is consistent with expectations for sodalite group minerals, which are synthesized under alkaline pH conditions (BRENCHLEY and WELLER, 1994). Hence, the dissolution rates should decline as the pH of the contacting solution is raised into the region where sodalite minerals are stable. In contrast, aluminosilicate minerals like nepheline show increasing dissolution rate with increasing pH (HAMILTON et al., 2001) and the data for Al, Na, and Si shown in Figure 7 generally reflect this behavior.
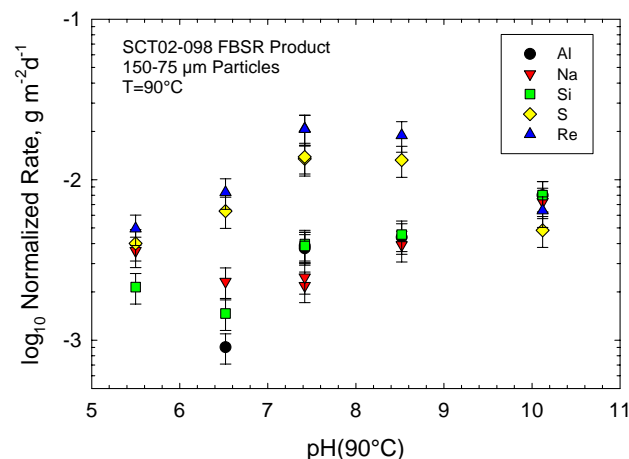
Figure 7. Normalized Release Rate as a Function of Solution pH in SPFT Experiments

3.3.5 Post-Test XRD Analyses

Figure 8 shows the results from XRD analyses of reacted samples after SPFT testing at 3 different pH values. The data show that nosean has dissolved below the detection limit of about 1-2 mass% in all the FBSR samples. Mass balance calculations show total sulfur loss at only about 70% of the initial mass after 23 days of testing so sulfate is being retained in the vessel. At pH(25°C) = 10 and 11, a hydrated hydroxysodalite appears to have replaced the nosean, probably through anion exchange of $2OH^-$ for SO_4^{2-} in the nosean. Diffusive mass transport from the interior of a microporous FBSR grain might then control how fast the released SO_4^{2-} enters bulk solution. At pH 7, hydroxysodalite is not stable and so dissolves as well, which is consistent with the trace amount detected by XRD (Figure 8).
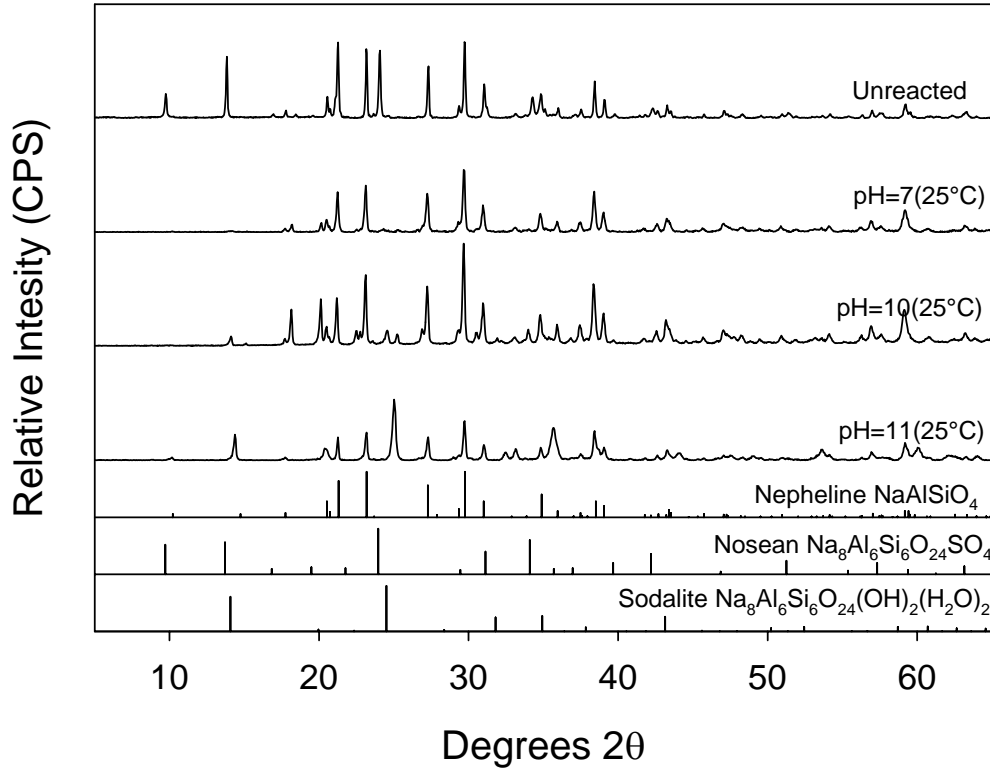
Figure 8. Post Test XRD Tracings of Reacted FBSR Product from SPFT Experiments

3.3.6 Nepheline Dissolution

If we make an assumption that S is present only in the nosean phase, an estimate of the dissolution rate of the nepheline phase in the FBSR product can be obtained by differencing. The results from this calculation are shown in Figure 9. The pH dependence of the rate (η) was calculated from a simple linear regression of the Si release data, excluding the datum at the lowest pH. The regressed value, $\eta = 0.25$, is significantly higher than the value ($\eta = 0.13$) reported by Tole et al. (1986) for nepheline dissolution at 80°C but less than the value for nepheline glass reported by Hamilton et al. (2001). However, our measured rates are much slower than those reported by Tole or Hamilton. Tole et al. (1986) report a nepheline dissolution rate at 80°C and pH 7 of 1.6 g m^{-2} d^{-1}, which is 800 times faster than the
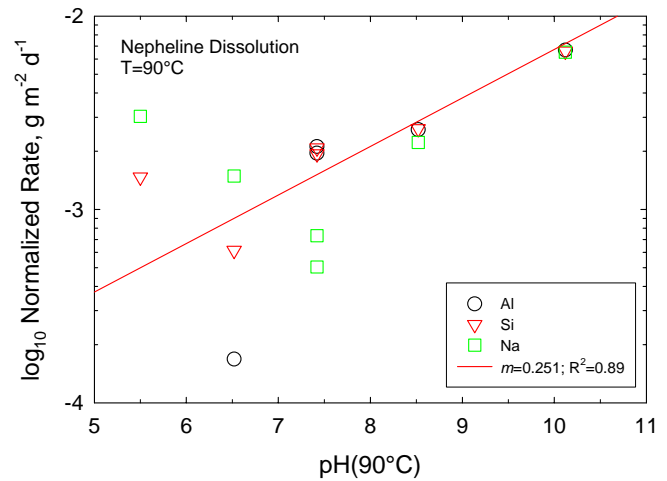
Figure 9. Calculated Normalized Release Rate for Nepheline Phase in FBSR Product as a Function of Solution pH in SPFT Experiments. Nepheline release rate was calculated by subtracting the normalized release rate of Al, Na, and Si release from nosean (based on S release) from the total measured release rate.

rates estimated from our SPFT data. The Tole et al. (1986) experiments were conducted with single crystals of nepheline cut with specific crystallographic orientation and Hamilton et al. (2001) used polished coupons of nepheline glass. However, the dissolution kinetics data of Tole and Hamilton agree to within about 35% at pH 11. Our data shows much slower reaction rates. Using the geometric surface area of the FBSR product to calculate the dissolution rate, our measured rates would still be nearly 7 times less than those of Tole et al. We can only speculate that substitution of Ti, Zr, and Fe into the nepheline structure has had a significant effect in lowering the dissolution rate of this phase from its relatively pure crystalline form.

4.0 PRESSURIZED UNSATURATED FLOW TESTS

In previous papers (MCGRAIL et al., 1997b; MCGRAIL et al., 2001d), equipment configurations for the patented (MCGRAIL et al., 1999) PUF system have been described. Briefly, the basic test apparatus consists of a column packed with crushed test material (or materials) of a known particle size and density, a computer data acquisition and control system, fluid pump, and electronic sensors. The column is fabricated from polyetheretherketone (PEEK), which is chemically inert so that dissolution reactions are not influenced by interaction with the column. A porous titanium plate with nominal pore size of 0.2 µm is sealed in the bottom of the column to ensure an adequate pressure differential for the conductance of fluid while operating under unsaturated conditions (Wierenga et al., 1993). Titanium was chosen because it is highly corrosion resistant and has excellent wetting properties. When water saturated, the porous plate allows water but not air to flow through it, as long as the applied pressure differential does not exceed the air entry relief pressure, or "bubble pressure," of the plate. The computer control system runs LabVIEW™ (National Instruments Corporation, Austin, Texas) software for logging test data to disk from several thermocouples, pressure sensors, inline sensors for effluent pH and conductivity. The column is suspended from an electronic strain gauge to accurately track water mass balance and saturation level. The column also includes a "PUF port," which is an electronically actuated valve that periodically vents the column gases. The purpose of column venting is to prevent reduction in the partial pressure of important gases, especially O_2 and CO_2, which may be consumed in a variety of chemical reactions.

4.1 MATERIALS

The material used was taken directly from the original sample of SCT02-098 and sieved to separate out the -10+20 mesh size fraction. No further sample preparation was done on this material. The specific surface area of the material was estimated from Equation (2) using a density of 2.76 g/cm^3 and applying a correction factor of 120 to account for the higher surface area of the actual material over the geometric. Consequently, the estimated specific surface area is 0.183 ±0.055 m^2/g.

4.2 TEST PROCEDURE

Two PUF experiments were performed at nominal flow rate of 2.0 mL/d and a temperature of 99°C. Each column was packed with the sieved FBSR product, giving an initial macroporosity of approximately 0.65 ±0.03, and then vacuum saturated with water at ambient temperature. A temperature controller was programmed to heat the column to 99°C in approximately 1 h (1°C/min). The column was allowed to initially desaturate during heating by gravity drainage and was also vented periodically to maintain an internal pressure less than the bubble pressure of the porous plate. After reaching 99°C, the influent valve was opened, and the syringe pump set to deliver influent at the specified flow rate. Column venting was set to occur once an hour. Effluent samples were collected in a receiving vessel, which was periodically drained into tared vials from which samples were extracted and acidified for elemental analysis by ICP-OES and ICP-MS.

4.3   RELEASE RATE AND ERROR CALCULATION

As in any flow-through column experiment, the calculation of kinetic rates from the effluent composition is slightly more involved than in simpler static experiments. The PUF experimental method introduces one additional complication, in that water content is also a variable that must be taken into account.

Most experiments using the PUF system are expected to be advection dominated. This can be demonstrated by computing a typical Peclet number for an experiment. The Peclet number (Pe) is given by

$$Pe = \frac{U_p x}{D} \tag{7}$$

where U_p is the pore velocity, x is the distance, and D is the molecular diffusion coefficient of water. In the current experiments, with a volumetric flow rate of 2 mL/d and water content (θ) during a test of approximately 0.3, a typical pore velocity in a PUF test is

$$U_p = \frac{Q}{\theta A} = \frac{(2.0 \text{ cm}^3/\text{d})(1.16 \times 10^{-5} \text{ d/s})}{(0.3)(2.85 \text{ cm}^2)} = 2.7 \times 10^{-5} \text{ cm/s} \tag{8}$$

where A is the cross-sectional area of the column.

For a column 7.62 cm in length and assuming $D = 10^{-5}$ cm^2/s, this gives a Pe number of

$$Pe = \frac{(2.7 \times 10^{-5})(3)(2.54)}{10^{-5}} = 20.6 \tag{9}$$

A system with Pe>4 is considered advection dominated, and so the PUF tests clearly fall in this category.

In an advection-dominated system, a 1-D steady state-mass balance for any constituent i is given simply by

$$U_d \frac{dc_i}{dx} = \theta \hat{r}_i \tag{10}$$

where U_d is the Darcy velocity (m/d), c_i is the concentration (g/m^3), θ is the volumetric water content, $\hat{r}_i$ is volumetric reaction rate (g m^{-3}·d^{-1}), and x is length (m). The volumetric reaction rate is given by

$$\hat{r}_i = \frac{f_i \dfrac{\theta}{\varepsilon} S r_i}{V_w} \tag{11}$$

where f_i is the mass fraction of element i, ε is porosity, S is the reactant surface area (m^2), r_i is the normalized release rate (g m^{-2} d^{-1}), and V_w is the volume of water in a representative elementary volume. It should be noted that in deriving Equation (11), we have assumed that surface area

contacted by condensed water is proportional to the degree of saturation in the column (θ/ε). Substituting Equation (11) into Equation (10), we have

$$U_d \frac{dc_i}{dx} = \frac{f_i \theta^2 S}{\varepsilon V_w} r_i .$$ (12)

Although it will not be demonstrated here, it is easy to show with typical values for the parameters in Equation (12) that solution is saturated with respect to amorphous silica and many other minerals within the first few millimeters of depth in the column. Consequently, we will assume that r_i is approximately constant as a function of distance along the flow path. If we further assume that volumetric water content is approximately uniform throughout the column, we can make use of the following identity

$$\frac{S}{V_w} = \frac{s \cdot m}{\theta V_c} = \frac{s(1-\varepsilon)\rho V_c}{\theta V_c} = \frac{s(1-\varepsilon)\rho}{\theta}$$ (13)

where s is the specific surface area of the particles (m^2/g), m is the total mass of the waste form in the column (g), V_c is the interior volume of the column (m^3), ρ is the bulk density (g/m^3) of the product. Substituting Equation (13) into Equation (12), we have

$$U_d \frac{dc_i}{dx} = \frac{f_i \theta s(1-\varepsilon)\rho}{\varepsilon} r_i.$$ (14)

Because the volumetric flow rate (Q, m^3/d) is fixed during a PUF test, the Darcy velocity is simply $U_d = \frac{4Q}{\pi d^2}$, where d is the column diameter. Integrating Equation (14), we have

$$\frac{4Q}{\pi d^2} \int_{c_{iB}}^{c_{iL}} dc_i = \frac{f_i \theta s(1-\varepsilon)\rho}{\varepsilon} r_i \int_0^L dx$$ (15)

where L is the column length, c_{iB} is the background concentration of element i, and c_{iL} is the concentration of element i in the effluent from the column. Rearranging the solution to Equation (15), we arrive at the expression we need to calculate normalized release rates from the effluent concentrations

$$r_i = \frac{4\varepsilon Q(c_{iL} - c_{iB})}{\theta s(1-\varepsilon)\rho \pi d^2 L f_i}$$ (16)

To calculate uncertainty in the release rates determined via Equation (16), a propagation of error analysis is performed. We make use of Equation (4) again and assume that uncertainty in the column diameter (d) and length (L) are small relative to the other parameters in Equation (16). Substituting (16) into Equation (4) gives

$$\sigma_{r_i} = r_i \sqrt{\left(\frac{\tilde{\sigma}_\varepsilon}{1-\varepsilon}\right)^2 + \left(\frac{\tilde{\sigma}_{c_{iL}}}{1-c_{iB}/c_{iL}}\right)^2 + \tilde{\sigma}_Q^2 + \tilde{\sigma}_\theta^2 + \tilde{\sigma}_s^2 + \tilde{\sigma}_\rho^2 + \tilde{\sigma}_{f_i}^2}$$ (17)

where the tilde over the σ symbol signifies the relative standard deviation for the subscripted parameter. In calculating the error bounds with Equation (17), we assumed the following fixed relative standard deviations:

$$\tilde{\sigma}_{\varepsilon} = 6\%, \tilde{\sigma}_{s} = 30\%, \tilde{\sigma}_{Q} = 2\%$$

$$\tilde{\sigma}_{\rho} = 5\%, \tilde{\sigma}_{c_{iL}} = 10\%, \tilde{\sigma}_{f_i} = 10\%$$

The value of $\tilde{\sigma}_{\theta}$ was calculated from the variation in water content recorded by the data acquisition system over the discrete interval between each fluid sampling. A computer macro program was written to perform this calculation directly in the Excel™ spreadsheet used to store the sensor data. Typically, errors in the calculated release rate from the PUF tests range from 55% to 38%.

4.4   RESULTS

The PUF tests were labeled PUF02A and PUF02B. Detailed results from effluent solution analyses from both tests are given in Appendix B. Because the tests were not run in identical fashion after the first 8 days (see below), the results will be discussed separately.

4.4.1   Sensor Data

Results from the computer-monitored test metrics for the PUF02A test are shown in Figure 10. As can be seen from the figure, the water content rose rapidly over the first 8 days of the

Figure 10. Computer Monitored Test Metrics From PUF Test A with SCT02-098 Steam Reformer Product. Pore plate became plugged after first seven days and was removed. The test was restarted without the plate.

test, whereupon the pore plate became plugged. The pore plate on the second test (PUF02B) became plugged at almost the same time. Both tests were halted. An examination of the pore plates revealed extensive deposits of a Pb-V rich phase that was identified by XRD as galena (PbS).

Because of concerns about repeated plugging of the pore plate, it was decided to restart the PUF02A test with the porous plate removed and allow gravity drainage alone to establish unsaturated flow conditions. We replaced the bottom cap with the same two port cap used on the top of the column. This allowed us to introduce air into the bottom of the column, which would flow up through the porous bed and out the top port. Thus, a continuous air flow at low pressure (0.2 psi) was established in this test. With the porous plate removed, oscillations in the water content appeared with an approximately constant period (see Figure 10). The oscillations in water content cause fluctuations in both the effluent pH and electrical conductivity. Attempts were made to adjust the air pressure to reduce the oscillations but these adjustments had no effect. The PUF02B test was treated differently as will be discussed in more detail below.

4.4.2 Effluent Analyses

Results from effluent chemical analysis from the PUF02A test are shown in Figure 11. In contrast with the SPFT data, Na release is the highest but declines with time in agreement with the electrical conductivity data. Also, there is some divergence between the release rates of S and Re after the test was stopped after 8 days. The divergence slowly disappears with time and becomes congruent after 20 days. It took approximately 1 week to reconfigure the test to run without the pore plate and precipitation of some sparingly soluble sulfides may have occurred during this period.

Figure 11. Normalized Concentrations of Na, S, and Re in Effluent From PUF Test A with Steam Reformer Product

Also plotted on Figure 11 is the calculated fractional release rate from LAWA44 glass based on B release. Boron is often used as an indicator element for glass dissolution because it is a major component of the borosilicate glass framework, and is highly soluble and does not typically get incorporated into secondary phases under most test conditions. Thus, it represents a conservative tracer for how fast radionuclides such as ^{99}Tc (or Re) can be released from the glass. Conversion to the fractional release rate normalizes out the differences in specific surface area of the particles used in the PUF test with LAWA44 glass and the FBSR product and so provides the best measure for comparison of the relative durability between the two waste forms. As can be readily observed in Figure 11, the fractional release rate of Re from the FBSR product and LAWA44 glass are identical within experimental error.

4.4.3 Water Content Distribution

After termination of the PUF test, the reacted solids were subsampled as found (loose and moist particles) at 5 mm intervals. These samples were analyzed for moisture content by drying in glass vials at 105°C until a constant mass was obtained. The results are shown in Figure 12. The data show relatively uniform water content for the first 55 mm and then the water content rises sharply. This water content distribution is atypical of distributions observed with reacted LAW glasses (McGRAIL et al., 2000b). Lack of a porous plate in the PUF02A test sets a water content boundary condition at the bottom of the column of 1 because the effluent line is positioned such that it remains water filled during the test. Water content very near 100%
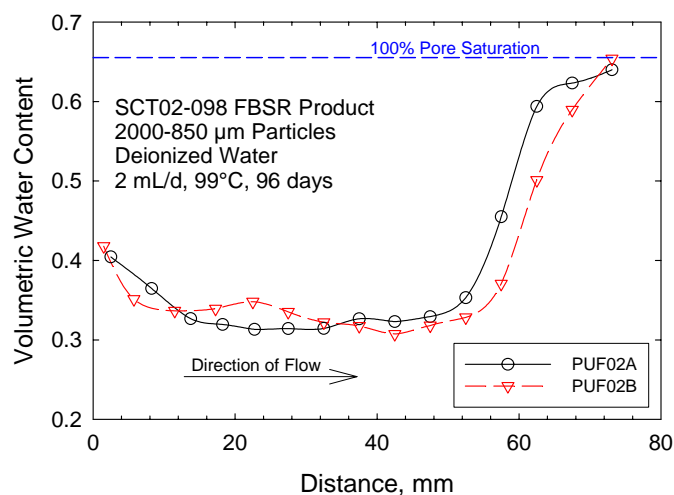
Figure 12. Water Mass Expressed as Volumetric Water Content as a Function of Column Depth in Post-Test PUF Samples

pore saturation is indeed observed at the very last sample, which is consistent with the imposed water saturation at the bottom of the column in this test. For the PUF02B test, the porous plate plugged at the end of the experiment and water contents reached near saturation values. Consequently, the moisture distribution from this test is similar to those obtained in the PUF02A test.

4.4.4 XRD/Raman Analyses

Results from XRD analyses of selected samples removed from the PUF column are shown in Figure 13. An important difference between the PUF test results and the SPFT test results is that nosean is detected in all the samples whereas this phase dissolved below detection levels in the SPFT experiments. Quantitative analyses of the XRD patterns was not possible but the change in height of the main 24° 2θ peak indicates slightly less nosean in the A1 sample than in the A8 and A15 samples. This is entirely consistent with expectations from advection-dominated reactive chemical transport. Solution packets moving through the PUF column become progressively more concentrated in Al, Na, Si, and S. Consequently, the dissolution rate of nosean should diminish with column depth. There is little difference in the amount of nosean remaining in the middle sample (A8) versus the bottom sample (A15). Solution saturation is apparently reached near the top of the column, which is consistent with the mathematical analysis discussed in Section 4.3. We also took a Raman spectrum from bottom sample A15, which is shown in Figure 1. The spectrum is virtually identical to the spectrum from the unreacted sample.
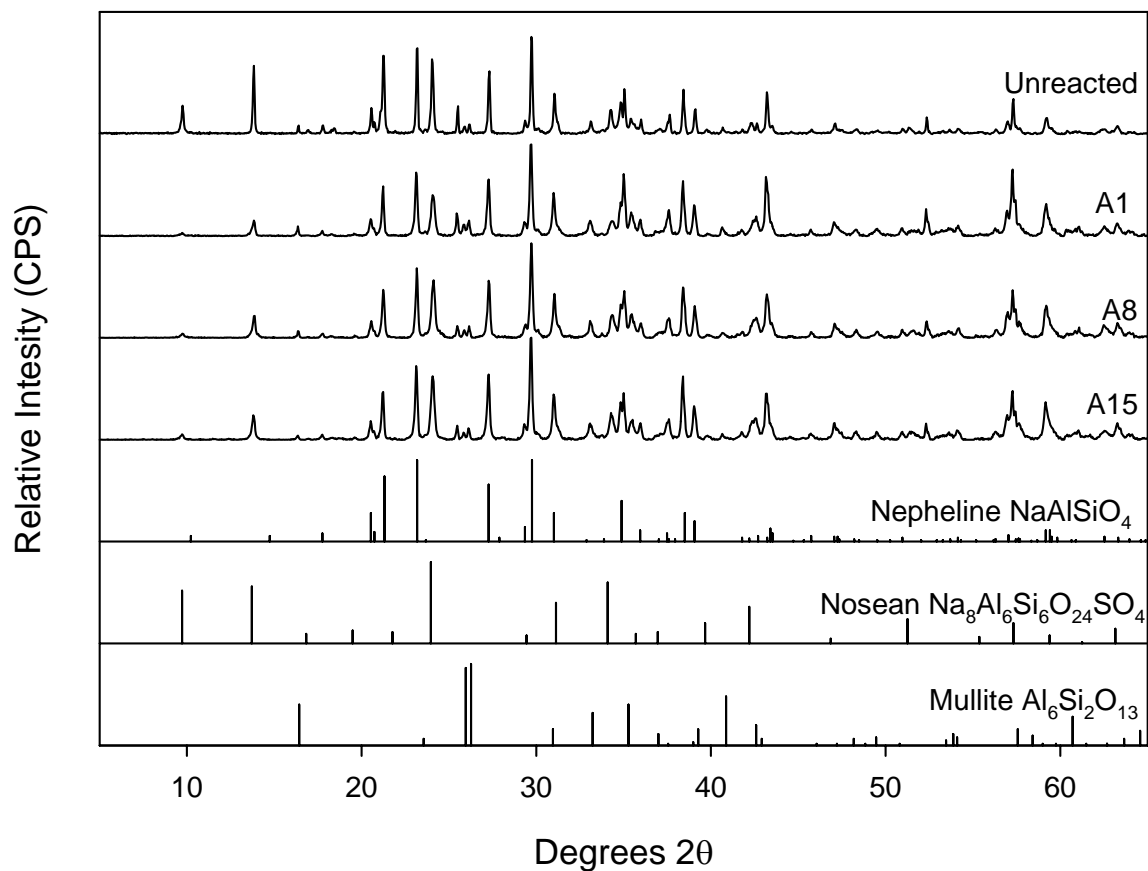
Figure 13. XRD Data for Unreacted and PUF Reacted FBSR Product. Samples labeled A1, A8, and A15 are from the top, middle, and bottom of the column, respectively. Minor amounts of hematite, magnetite, and corundum were also detected in addition to the phases shown.

4.4.5 PUF02B Test Results

For the PUF02B test, which also plugged after the first 8 days of testing, the column was flushed with 20 pore volumes of deionized water to help remove any ultrafine particles that could cause the plate to plug. The test was then restarted with a new porous plate. Output from the computer-monitored sensors is shown in Figure 14. The column flushing significantly reduced the effluent electrical conductivity and pH after the test was restarted with a nominal flow rate of 2 mL/d. The plate plugged again at 45, and 60 days, and just before the test was terminated. The plate was replaced each time and the test restarted (except at the end of the test).
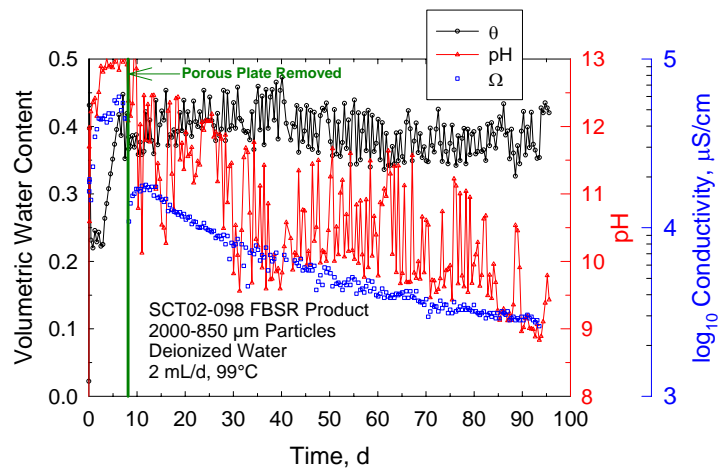

Figure 14. Computer Monitored Test Metrics From PUF Test B with SCT02-098 Steam Reformer Product. Pore plate became plugged repeatedly during the test and was replaced.

Despite the less than optimal run conditions of this test, the effluent chemical analyses (Figure 15) show remarkably consistent results with the PUF02A test. In fact, the Re release rate at the end of the test is identical within experimental error to the values obtained for the PUF02A test (Figure 11).

XRD and SEM analyses of the reacted solids from this test were also virtually identical with the results obtained from the PUF02A samples. Nosean was identified in all the reacted samples. Samples taken from the middle and bottom of the column show evidence for a crystalline secondary phase formed on the outer surface

Figure 15. Normalized Concentrations of Na, S, and Re in Effluent From PUF Test B with Steam Reformer Product

of the FBSR particles. The chemistry, determined from energy dispersive spectroscopy, and morphology of this phase are similar to gmelinite [$(Na_2,Ca)Al_2Si_4O_{12} \cdot 6H_2O$]. Gmelinite is a common alteration phase observed in PUF reacted samples of ILAW glasses. Powder XRD data, however, are inconclusive with respect to the presence of this phase in the reacted FBSR samples and the alteration phase could be any of a number of hydrous zeolites.

4.8

Figure 16. SEM Micrographs of PUF Reacted FBSR
Grain from the Middle Region of the Column

Page left intentionally blank.

5.0   DISCUSSION

One of the key objectives of the work described in this report was to provide a preliminary assessment of the performance of the FBSR product relative to the well-documented behavior of ILAW glasses. While insufficient data were generated in this initial work to support a complete disposal system analysis for the FBSR product as has been done for ILAW glass (BACON et al., 2002), it is possible to directly compare the relative performance of the FBSR product in the laboratory tests to ILAW glass, which has been tested under essentially identical conditions.

5.1.1   Bounding Case Based on SPFT Experiments

The SPFT test is designed to provide information on waste form dissolution mechanisms and kinetic rate law constants that is not readily obtained by any other experimental method (MCGRAIL et al., 2000a). As the test is completely water saturated and typically run at quite high flow rate, the test is not intended and certainly does not represent a typical vadose zone environment at Hanford. However, the data can be used to provide an absolute upper bound on release rates and because pH is fixed and solution chemistry effects are minimized, the test provides a straightforward means to compare the relative durability of waste forms under extreme conditions (relative to expected environmental conditions at the ILAW facility).

In contrast with the behavior of silicate glasses, Re release rate data for the FBSR product (Figure 7) show very little pH dependence. In fact, Re release actually decreases from pH 10 to 11. As was discussed previously, we believe this reflects the greater stability of sodalite group minerals at alkaline pH. Rhenium release rates determined in the SPFT experiments can be compared with published data on ILAW glasses. The normalized release rates are approximately 100 times *slower* than LD6-5412 glass at pH 9 and 90°C (MCGRAIL et al., 1997a) and about the same as LAWA44 glass at pH 9 but at 26°C (MCGRAIL et al., 2001b). However, the reader is cautioned that this does not imply lower overall release rates for the disposal system. As noted above, the specific surface area of the FBSR product is about 120 times larger than the specific surface area for glass of identical particle size.[a] Thus, a first order comparison of the test results indicates approximately the same total mass flux of Re (Tc) would be released from the FBSR product and ILAW glass. However, this comparison does not correctly represent the relative surface areas per unit volume in a waste package. In an ILAW waste package, our current working assumption is that cracking induced from thermal stresses during cooldown will increase the glass surface by about a factor of 10 over the geometric surface area (MCGRAIL et al., 2001c). Thus, for every 1 m^3 of glass, there is approximately 60 m^2 of glass surface area giving an effective glass surface area to volume ratio (S/V) of approximately 60 m^{-1}. If we assume a particle size of 4 mm to 1 mm diameter for the final FBSR product, Equation (2) gives an estimate of the geometric surface area of 0.001 m^2/g. Assuming a packing efficiency of 35% (consistent with our measured bulk porosity), the effective product density is 1×10^6 g/m^3. Multiplying these two values together, we arrive at a S/V ratio for an FBSR product waste package of 1000 m^{-1}. This is 16 times larger than the S/V for glass. However, we noted above that geometric surface area is probably not an appropriate estimate of the actual product surface area. BET measurements indicate a value 120 times larger. Using the BET value, the effective S/V ratio for a FBSR waste package would be 2000 times larger than a glass waste package. Since our measured normalized

---

[a]McGrail et al. (1997a) conclusively showed that geometric surface area is the appropriate measure to use for calculating dissolution rates for glass particles prepared via the ASTM PCT method, not a BET measured surface area.

release rate is 100 times less than glass, we arrive at a final estimate of the radionuclide flux for a FBSR waste package that is about 20 times larger than for an ILAW glass waste package.

It is critically important to remember that our estimate above is a bounding release rate estimate and completely neglects the effects of solution chemistry in potentially slowing the release rate as water percolates through a waste package. The PUF experimental data provide some insight into these effects and will be discussed next. We have also neglected any differences in water content that may arise due to differing hydraulic conductivity and water retention characteristics for the FBSR product versus glass. We discuss this effect in more detail in Section 5.1.3. Finally, a very important uncertainty remains in extrapolating our experimental data, taken at 90°C, down to the disposal system temperature of approximately 15°C. Extensive experimental data is available for ILAW glasses that provide a well-defined activation energy for making this temperature extrapolation. Although we would *expect* similar temperature dependence for the silicate minerals in the FBSR product, we have not conducted the necessary temperature-dependent experiments in this preliminary work to make an extrapolation possible. **Consequently, it is impossible to directly assess the relative performance of the FBSR product to glass at disposal system conditions at this time. The 20X higher release rate estimated from the 90°C data may or may not accurately reflect relative performance at 15°C and so can only be viewed as a single datum with considerable uncertainty with respect to disposal system behavior.** For example, if the rate controlling mechanism for the release of Re is diffusive mass transfer from the interior of the microporous particles, the activation energy for this mechanism will be much smaller than for a chemical reaction (bond-breaking) mechanism that controls release rates from silicate glasses. The result would be a significantly smaller decrease in release rate with temperature and so >20X higher relative rate of release at 15°C for the FBSR product as compared with ILAW glass.

If the temperature-dependence of the release rate is similar to ILAW glasses, a 20X higher release rate for a bounding case scenario would *not* compromise the overall performance of the ILAW disposal system. Results from the 2001 ILAW Performance Assessment indicate several orders of magnitude margin in terms of meeting groundwater protection criteria (MANN et al., 2001). Since the FBSR product would represent only a fraction of the total disposed ILAW, a 20 times higher release rate would not significantly impact the overall radionuclide release rate from the disposal system. However, because of the highly nonlinear behavior of the disposal system as a whole, confirmation of this analysis is required through the same rigorous methods used for ILAW glass (BACON and MCGRAIL, 2001).

5.1.2 Relative Performance in PUF Experiments

As shown in Figure 11 and Figure 15, a comparison of the fractional release rate for the FBSR product with LAWA44 glass in the PUF test shows identical performance (at the longest reaction times we tested) within experimental error. As the PUF experiment more accurately simulates a vadose zone environment, these test data provide better insight with respect to expected product performance than does the SPFT test. We also note that nosean remained in the PUF reacted samples whereas this phase dissolved below detection limits in the water-saturated SPFT experiments. In part, this is due to the fact that FBSR grains are partially wetted in the PUF experiment and so it would be expected that portions of the original phase assemblages in the product would remain. However, again, this also more accurately reflects the expected hydraulic behavior in a real disposal system.

The conclusion from the PUF tests is unequivocal in that performance of the FBSR product is equivalent to glass under the same test conditions. However, we cannot conclude from these test data alone that performance under disposal system conditions will also be equivalent to glass. The same issues discussed above with respect to temperature dependence of the release rate are issues in the PUF experiments. Again, although we would expect from first principles considerations that release rates from the FBSR product will slow with decreasing temperature, insufficient data presently exists to make the extrapolation down to 15°C. Until additional temperature-dependent experimental data are available, we cannot assess the relative performance of the FBSR product to glass in a disposal system environment. **Still, the PUF experimental data provide no indication that FBSR product would be an unacceptable ILAW form.**

5.1.3   Hydraulic Behavior of FBSR Waste Packages

Hydraulic properties are an often overlooked factor that can significantly affect waste form performance in a vadose zone environment. Space between waste packages in the ILAW facility is planned to be filled with backfill soil (BURBANK, 2001) that is of smaller particle size and lower bulk porosity than expected for FBSR product (based on the SCT02-098 sample examined in this report). The physics of unsaturated flow (BEAR, 1972) dictate that larger pores drain first in an unsaturated porous medium and so the FBSR product should act as a hydraulic barrier to fluid flow.

To test this hypothesis, flow simulations were conducted with the Subsurface Transport Over Multiple Phases (STOMP) code (WHITE and OOSTROM, 2000). Simulations were based on those performed for the 2001 ILAW PA (MANN et al., 2001). For the FBSR product, macroporosity was estimated at 50% and particle size was assumed to follow a Gaussian distribution with maximum and minimum particle size of 4- and 1-mm diameter, respectively. This particle size corresponds to coarse sand to gravel porous medium according to the USDA classification. Microporosity within each individual particle was estimated from mercury porosimetry analyses provided by Hazen Research, Inc. Mean pore diameter was 0.9 µm, which corresponds to clay size particles according to the USDA classification.

Based on the pore size estimates given above, laboratory-measured hydraulic properties for a gravel (ROCKHOLD et al., 1993) were assumed for the FBSR product's macroporosity, and laboratory-measured hydraulic properties for a clay (MUALEM, 1976) were assumed for the FBSR

Table 3. Hydraulic Properties used in Flow Simulations of FBSR Product

Material	Porosity	Residual Saturation	van Genuchten α, cm^{-1}	van Genuchten n	Saturated Hydraulic Conductivity, cm s^{-1}
FBSR Macroporosity	0.518	2.7×10^{-2}	3.54	2.66	1.85
FBSR Microporosity	0.450	3.1×10^{-3}	0.042	2.70	9.5×10^{-7}
Backfill	0.316	0.155	0.035	1.72	1.9×10^{-3}
Hanford Sand	0.375	0.109	0.055	1.77	2.9×10^{-3}

product's microporosity. Hydraulic properties for the surrounding materials in the ILAW trench were the same as values used for the 2001 ILAW PA. Waste package size and layout was also assumed the same as in the 2001 ILAW PA.

Two simulations were conducted. In the first, microporosity of the particles was ignored and only the single set of hydraulic properties was assumed for the FBSR product corresponding to the macroporosity entry in Table 3. In the second simulation, a dual porosity model for the FBSR product was used. In the dual-porosity model, hydraulic properties for both macropores and internal microporosity given in Table 3 were included in the simulation.

Moisture Content: 0.020 0.027 0.040 0.054 0.067 0.080 0.093 0.106 0.120 0.133 0.146
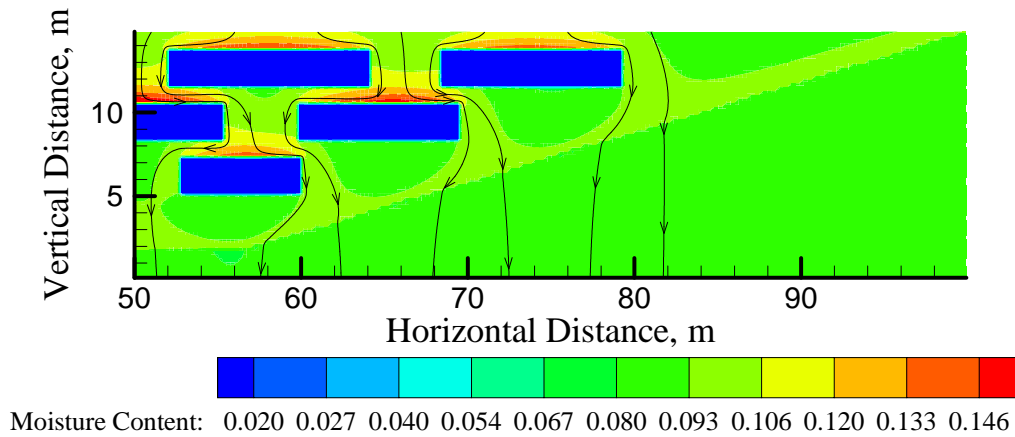
Figure 17. Flow Field Surrounding FBSR Product for Single-Porosity Simulation

Moisture Content: 0.020 0.027 0.040 0.054 0.067 0.080 0.093 0.106 0.120 0.133 0.146
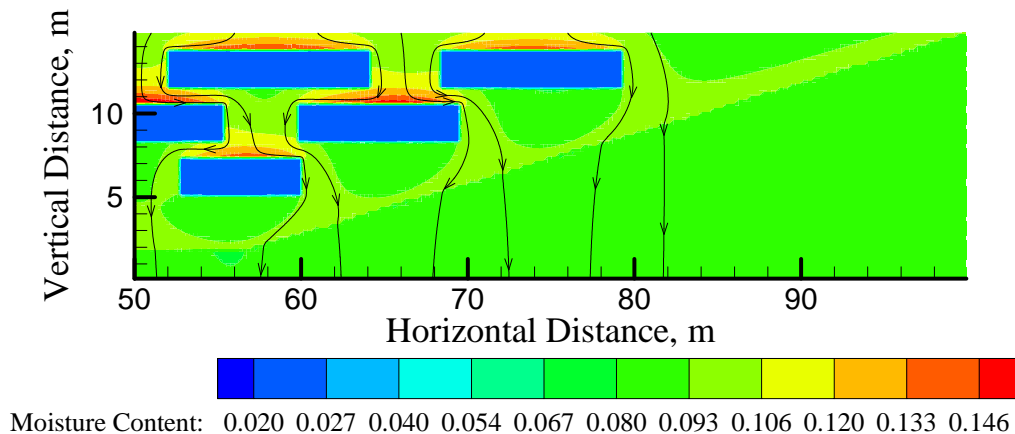
Figure 18. Flow Field Surrounding FBSR Product for Dual-Porosity Simulation

Results for the single-porosity simulation are shown in Figure 17. Most of the infiltrating water is diverted around the waste packages containing the FBSR product, which remain significantly drier relatively to the surrounding soil. Water contents in the interior of the waste packages are an approximately constant 0.014. This simulation confirms our hypothesis regarding the hydraulic barrier effect of the FBSR form. Results from the dual-porosity simulation (Figure 18) are similar except that moisture content in the interior of the waste packages is 50% higher in the dual-porosity simulation (0.021). The additional moisture is contained in the micropores of the FBSR grains. However, the macroscopic flow paths are virtually identical for the two simulations. Because the clay-like matrix has a permeability that is 6 orders of magnitude less than the macropores, the macropores control the flow through the disposal system.

6.0   CONCLUSION

A single sample of FBSR product has been analyzed and tested using single-pass flow through (SPFT) and pressurized unsaturated flow (PUF) methods. The FBSR product was found to consist of two primary mineral phases, nepheline and nosean. Inference from synthesis of perrhenate sodalite and the 1:1 tracking of S of Re release from the product in SPFT tests suggests that Re, a chemical analog for ^{99}Tc, is most likely partitioned to the nosean phase. Results from the SPFT tests, which conservatively bound maximum release rates, show little pH dependence on the release rate of Re and in fact declining release rate at pH(90°C) > 8. Dissolution rates for the nepheline phase show conventional pH rate dependence with increasing rate as a function of pH. The SPFT data were used to calculate a bounding release rate for a FBSR waste package and compared with the available data from ILAW glasses. The bounding case release rates are about 20 times higher for the FBSR product as compared with glass. However, because of uncertainty regarding the true reactive surface area of the product, actual differences in release rate at 90°C probably range between 2 to 20 times higher than ILAW glass. Additional testing is needed to determine relative bounding rates at actual disposal system conditions (15°C), irrespective of reactive surface area assumptions. Fractional release rates, again based on Re release, calculated from PUF experiments with the FBSR product show essentially identical performance with a reference ILAW glass (LAWA44) tested under the same conditions. However, the temperature dependence of the measured rate is not known and so the relative rates at 15°C cannot be estimated at this time. Assuming similar activation energy to glass for the temperature dependence of the dissolution kinetics of the primary silicate phases, the FBSR product performance appears to be approximately equivalent to ILAW glass. Additional testing is needed to reach a scientifically defensible conclusion regarding actual FBSR product performance based on rigorous disposal system simulations equivalent to what as has been done for ILAW glasses. Still, all the presently available experimental data suggest that FBSR product would be an adequate alternative ILAW form that merits further study.

Page left intentionally blank.

7.0 RECOMMENDATIONS FOR ADDITIONAL WORK

As was mentioned in the Conclusion section, a priority need is to develop the necessary data to support completion of a preliminary disposal system performance assessment for the FBSR product. The STORM reactive chemical transport model has been used to generate the source-term for ILAW glass (BACON and MCGRAIL, 2001) and the same code can be used for an analysis of the FBSR product. To accomplish this, the following input data need to be generated:

- Temperature dependence of release rate from the FBSR product
- Kinetic rate law constants for nosean
- Kinetic rate law constants for nepheline
- Solubility product for nosean
- Solubility product for nepheline (confirmation of literature values only)
- Partitioning coefficient of Tc between primary phases in FBSR product
- Hydraulic properties for FBSR product
- Secondary phases formed from FBSR corrosion

Generating these data will require additional testing of FBSR product(s) using similar methods as has been discussed in this report. Development of kinetic rate law and solubility product data for nosean and nepheline will also require synthesizing these phases, verifying their chemical and crystal structure, and then performing the necessary suite of tests. Partitioning of Tc among the phases in the FBSR product is an important question. Test results from the SCT02-098 sample analyzed in this report suggest that Re is primarily present in the nosean phase. Although we have synthesized perrhenate sodalite, pertechnetate sodalite needs to be synthesized and the structure confirmed. Production of a mixed perrhenate/pertechnetate and sulfate form of nosean should also be performed. Finally, FBSR product should be produced with significantly higher concentrations of Re to confirm the formation of a mixed perrhenate/sulfate sodalite during the FBSR process.

There is also a need to conduct some test method development work with respect to the PUF test. Pore plate plugging was a significant problem that should be remedied in future tests. Possible solutions include running the experiment without a porous plate (as was done for one test in this report), and evaluating different pore plates with larger pore sizes and perhaps different materials.

Page left intentionally blank.

8.0   REFERENCES

Aagaard, P. and H. C. Helgeson. 1982. "Thermodynamic and Kinetic Constraints on Reaction Rates Among Minerals and Aqueous Solutions. I. Theoretical Considerations." *Am. J. Sci.* **282**:237-285.

Abel, K. H. 2002. *Initial Suitability Evaluation of Steam-Reformed LAW for Direct Land Disposal.* 24590-LAW-TSP-RT-02-007, Rev 0, Bechtel National, Inc., Richland, Washington.

Anbeek, C., N. Vanbreemen, E. L. Meijer, and L. Vanderplas. 1994. "The Dissolution of Naturally Weathered Feldspar and Quartz." *Geochim. Cosmochim. Acta* **58**(21):4601-4613.

Bacon, D. H. and B. P. McGrail. 2001. *Waste Form Release Calculations for the 2001 Immobilized Low-Activity Waste Performance Assessment.* PNNL-13369, Pacific Northwest National Laboratory, Richland, Washington.

Bacon, D. H., B. P. McGrail, V. L. Freedman, G. Ventura, P. Risoluti, and K. M. Krupka. 2002. "Performance Assessment of Low-Level Waste Disposal Facilities Using Coupled Unsaturated Flow and Reactive Transport Simulators." *Mat. Res. Soc. Symp. Proc.* **713**:267-274.

Bear, J. 1972. *Dynamics of Fluids in Porous Media.* American Elsevier.

Brantley, S. L. and N. P. Mellott. 2000. "Surface Area and Porosity of Primary Silicate Minerals." *Am. Mineral.* **85**:1767–1783.

Brenchley, M. E. and M. T. Weller. 1994. "Synthesis and Structures of $M_8[AlSiO_4]_6 \cdot (XO_4)_2$, M = Na, Li, K; X = Cl, Mn Sodalites." *Zeolites* **14**:1994.

Brunauer, S., P. H. Emmett, and E. Teller. 1938. "Adsorption of Gases in Multimolecular Layers." *J. Physical Chem.* **60**:309-319.

Burbank, D. A. 2001. *Conceptual Design Report for the Immobilized Low-Activity Waste Disposal Facility, Project W-520.* RPP-7908, Revision 0, CH2M Hill Hanford Group, Inc., Richland, Washington.

Fogler, H. S. 1986. *Elements of Chemical Reaction Engineering.* Prentice Hall.

Hamilton, J. P., S. L. Brantley, C. G. Pantano, L. J. Criscenti, and J. D. Kubicki. 2001. "Dissolution of Nepheline, Jadeite and Albite Glasses: Toward Better Models for Aluminosilicate Dissolution." *Geochim. Cosmochim. Acta* **65**(21):3683-3702.

Jantzen, C. M. 2002. *Engineering Study of the Hanford Low Activity Waste (LAW) Steam Reforming Process.* WSRC-TR-2002-00317, Rev. 0, Westinghouse Savannah River Company, Aiken, South Carolina.

Jeong, S.-Y., L. R. Morss, and W. L. Ebert. 2002. "Corrosion of Glass-Bonded Sodalite and Its Components as a Function of pH and Temperature." *Mat. Res. Soc. Symp. Proc.* **713**:413-420.

Knauss, K. G., W. L. Bourcier, K. D. McKeegan, C. I. Merzbacher, S. N. Nguyen, F. J. Ryerson, D. K. Smith, H. C. Weed, and L. Newton. 1990. "Dissolution Kinetics of a Simple Analogue Nuclear Waste Glass as a Function of pH, Time and Temperature." *Mat. Res. Soc. Symp. Proc.* **176**:371-381.

Mann, F. M., R. J. Puigh, II, S. H. Finfrock, E. J. Freeman, R. Khaleel, D. H. Bacon, M. P. Bergeron, B. P. McGrail, S. K. Wurstner, K. Burgard, W. R. Root, and P. E. LaMont. 2001. *Hanford Immobilized Low-Activity Tank Waste Performance Assessment: 2001 Version.* DOE/ORP-2000-24 Rev. 0, U.S. Department of Energy, Richland, Washington.

Matson, D. W., S. K. Sharma, and J. A. Philpotts. 1986. "Raman-Spectra of Some Tectosilicates and of Glasses Along the Orthoclase-Anorthite and Nepheline-Anorthite Joins." *Am. Mineral.* **71**(5-6):694-704.

Mattigod, S. V., B. P. McGrail, D. M. McCready, and K. E. Parker. 2002. "Synthesis and Structure of Perrhenate Sodalite." *J. Phys. Chem. B* **In press**.

McGrail, B. P., D. H. Bacon, W. L. Ebert, and K. P. Saripalli. 2000a. *A Strategy to Conduct an Analysis of the Long-Term Performance of Low-Activity Waste Glass in a Shallow Subsurface Disposal System at Hanford.* PNNL-11834 Rev. 1, Pacific Northwest National Laboratory, Richland, Washington.

McGrail, B. P., D. H. Bacon, J. P. Icenhower, F. M. Mann, R. J. Puigh, H. T. Schaef, and S. V. Mattigod. 2001a. "Near-Field Performance Assessment for a Low-Activity Waste Glass Disposal System: Laboratory Testing to Modeling Results." *J. Nuc. Mat.* **298**(1-2):95-111.

McGrail, B. P., W. L. Ebert, A. J. Bakel, and D. K. Peeler. 1997a. "Measurement of Kinetic Rate Law Parameters on a Na-Ca-Al Borosilicate Glass for Low-Activity Waste." *J. Nuc. Mat.* **249**:175-189.

McGrail, B. P., J. P. Icenhower, D. H. Bacon, H. T. Schaef, P. F. Martin, E. A. Rodriguez, and J. L. Steele. 2001b. *Low-Activity Waste Glass Studies: FY2001 Summary Report.* PNNL-13761, Pacific Northwest National Laboratory, Richland, Washington.

McGrail, B. P., J. P. Icenhower, D. H. Bacon, J. D. Vienna, K. P. Saripalli, H. T. Schaef, P. F. Martin, R. D. Orr, E. A. Rodriguez, and J. L. Steele. 2002. *Low-Activity Waste Glass Studies: FY2002 Summary Report.* PNNL-14145, Pacific Northwest National Laboratory, Richland, Washington.

McGrail, B. P., J. P. Icenhower, P. F. Martin, D. R. Rector, H. T. Schaef, E. A. Rodriguez, and J. L. Steele. 2000b. *Low-Activity Waste Glass Studies: FY2000 Summary Report.* Pacific Northwest National Laboratory, Richland, Washington.

McGrail, B. P., J. P. Icenhower, P. F. Martin, H. T. Schaef, M. J. O'Hara, E. A. Rodriguez, and J. L. Steele. 2001c. *Waste Form Release Data Package for the 2001 Immobilized Low-Activity Waste Performance Assessment.* PNNL-13043 Rev. 2, Pacific Northwest National Laboratory, Richland, Washington.

McGrail, B. P., P. F. Martin, and C. W. Lindenmeier. 1997b. "Accelerated Testing of Waste Forms Using a Novel Pressurized Unsaturated Flow (PUF) Method." *Mat. Res. Soc. Symp. Proc.* **465**:253-260.

McGrail, B. P., P. F. Martin, and C. W. Lindenmeier. 1999. *Method and Apparatus for Measuring Coupled Flow, Transport, and Reaction Processes Under Liquid Unsaturated Flow Conditions.* Patent No. 5974859, Battelle Memorial Institute, USA.

McGrail, B. P., P. F. Martin, C. W. Lindenmeier, and H. T. Schaef. 2001d. Application of the Pressurised Unsaturated Flow (PUF) Test for Accelerated Ageing of Waste Forms. In *Ageing Studies & Lifetime Extension of Materials* (ed. L. G. Mallinson), pp. 313-320. Kluwer Academic/Plenum Publishers, New York.

Morss, L. R., M. L. Stanley, C. D. Tatko, and W. L. Ebert. 2000. "Corrosion of Glass-Bonded Sodalite as a Function of pH and Temperature." *Mat. Res. Soc. Symp. Proc.* **608**:733-738.

Mualem, Y. 1976. *A Catalogue of the Hydraulic Properties of Unsaturated Soils.* Research Project 442, Technion, Israel Institute of Technology, Haifa, Israel

Rockhold, M. L., M. J. Fayer, and P. R. Heller. 1993. *Physical and Hydraulic Properties of Sediments and Engineered Materials Associated with Grouted Double-Shell Tank Waste Disposal at Hanford.* PNL-8813, Pacific Northwest National Laboratory, Richland, Washington.

Tole, M. P., A. C. Lasaga, C. Pantano, and W. B. White. 1986. "The Kinetics of Dissolution of Nepheline ($NaAlSiO_4$)." *Geochim. Cosmochim. Acta* **50**(3):379-392.

Westerterp, K. R., W. P. M. van Swaaij, and A. A. C. M. Beenackers. 1983. *Chemical Reactor Design and Operation*. John Wiley and Sons.

White, M. D. and M. Oostrom. 2000. *STOMP - Subsurface Transport Over Multiple Phases Version 2.0, Theory Guide.* PNNL-12030, Pacific Northwest National Laboratory, Richland, Washington.

Wierenga, P. J., M. H. Young, G. W. Gee, R. G. Hills, C. T. Kincaid, T. J. Nicholson, and R. E. Cady. 1993. *Soil Characterization Methods for Unsaturated Low-Level Waste Sites.* PNL-8480, Pacific Northwest Laboratory, Richland, Washington.

Wolery, T. J. 1992. *EQ3NR, A Computer Program for Geochemical Aqueous Speciation-Solubility Calculations: Theoretical Manual, User's Guide, and Related Documentation (Version 7.0).* UCRL-MA-110662 PT III, Lawrence Livermore National Laboratory, Livermore, California.

Page left intentionally blank.

APPENDIX A – SPFT TEST DATA

Table A1. SPFT pH Sweep Experimental Conditions and Dissolutions Rates

Sample I.D.	Duration day	pH (25°C)	Target Flow rate mL d^{-1}	Actual Flow rate mL d^{-1}	^{a}C$_{Al}$ µg L^{-1} [10]^c	C$_{Si}$ mg L^{-1} [0.10]	C$_{Na}$ mg L^{-1} [0.10]	C$_S$ µg L^{-1} [50]	C$_{Re}$ µg L^{-1} [0.1]	^{b}Rate Al g m^{-2} d^{-1}	Rate Si g m^{-2} d^{-1}	Rate Na g m^{-2} d^{-1}	Rate S g m^{-2} d^{-1}	Rate Re g m^{-2} d^{-1}
Cell SCT2-1														
SCT2-1A	na	nm	60	nm	7.9	0.02	0.03	110	0.012	na	na	na	na	na
SCT2-1B	na	nm	60	nm	8.6	0.02	0.04	97	0.012	na	na	na	na	na
SCT2-1C	na	nm	60	nm	13.3	0.03	0.05	103	0.012	na	na	na	na	na
SCT2-1.1	1.00	7.46	60	58	1122	15	157	1145	3.14	3.17E-04	4.20E-03	4.84E-02	1.36E-02	2.68E-02
SCT2-1.2	1.84	7.34	60	38	552	13	94	2247	4.55	1.03E-04	2.46E-03	1.91E-02	1.85E-02	2.58E-02
SCT2-1.3	3.11	7.25	60	62	529	8.9	58	1521	2.67	1.58E-04	2.61E-03	1.90E-02	1.97E-02	2.43E-02
SCT2-1.6	10.29	7.11	60	55	262	7.1	21	1241	2.20	6.80E-05	1.86E-03	6.03E-03	1.40E-02	1.77E-02
SCT2-1.11	13.02	7.25	60	73	181	7.2	15	1002	1.82	6.12E-05	2.49E-03	5.92E-03	1.47E-02	1.94E-02
SCT2-1.14	16.07	7.08	60	57	199	10	20	1081	2.01	5.28E-05	2.76E-03	6.12E-03	1.25E-02	1.68E-02
SCT2-1.17	19.13	7.06	60	41	186	10	18	836	1.41	3.58E-05	1.98E-03	3.97E-03	6.79E-03	8.52E-03
SCT2-1.20	20.12	7.04	60	68	153	8.8	14	515	0.790	4.77E-05	2.85E-03	4.88E-03	6.27E-03	7.81E-03
SCT2-1.21	21.09	7.03	60	36	161	10	16	572	0.910	2.67E-05	1.72E-03	3.10E-03	3.79E-03	4.78E-03
SCT2-1.22	22.05	6.99	60	72	146	7.7	12	424	0.595	4.82E-05	2.64E-03	4.45E-03	5.19E-03	6.20E-03
SCT2-1.23	23.00	7.05	60	52	154	8.4	12	365	0.520	3.66E-05	2.06E-03	3.28E-03	3.03E-03	3.88E-03
Cell SCT2-2														
SCT2-2A	na	nm	70	nm	13	0.07	0.05	106	0.012	na	na	na	na	na
SCT2-2B	na	nm	70	nm	7.3	0.07	0.04	102	0.012	na	na	na	na	na
SCT2-2C	na	nm	70	nm	7.8	0.07	0.06	101	0.012	na	na	na	na	na
SCT2-2.1	1.00	8.31	70	72	7090	13.0	107	653	1.63	2.50E-03	4.43E-03	4.08E-02	8.88E-03	1.72E-02
SCT2-2.2	1.84	8.26	70	44	5311	10	56	256	0.399	1.14E-03	2.14E-03	1.31E-02	1.50E-03	2.50E-03
SCT2-2.3	3.11	8.16	70	71	4972	9.3	36	514	1.24	1.72E-03	3.11E-03	1.34E-02	6.50E-03	1.28E-02
SCT2-2.6	10.29	8.19	70	73	4208	7.6	15	1088	2.03	1.51E-03	2.63E-03	5.99E-03	1.62E-02	2.19E-02
SCT2-2.11	13.02	8.32	70	53	3936	7.1	15	1126	2.11	1.03E-03	1.79E-03	4.15E-03	1.22E-02	1.65E-02
SCT2-2.14	16.07	8.15	70	78	4025	7.2	13	940	1.43	1.54E-03	2.66E-03	5.30E-03	1.47E-02	1.64E-02
SCT2-2.17	19.13	8.09	70	43	3354	5.7	9.8	812	1.39	7.07E-04	1.15E-03	2.22E-03	6.85E-03	8.76E-03
SCT2-2.20	20.12	8.08	70	73	2890	5.0	7.3	616	1.04	1.04E-03	1.71E-03	2.83E-03	8.44E-03	1.11E-02
SCT2-2.21	21.09	8.09	70	50	2957	5.1	7.7	627	1.08	7.27E-04	1.21E-03	2.05E-03	5.90E-03	7.92E-03

Table A1. SPFT pH Sweep Experimental Conditions and Dissolutions Rates

Sample I.D.	Duration day	pH (25°C)	Target Flow rate mL d⁻¹	Actual Flow rate mL d⁻¹	$^a C_{Al}$ µg L⁻¹ [10]^c	C_{Si} mg L⁻¹ [0.10]	C_{Na} mg L⁻¹ [0.10]	C_S µg L⁻¹ [50]	C_{Re} µg L⁻¹ [0.1]	^{b}Rate Al g m⁻² d⁻¹	Rate Si g m⁻² d⁻¹	Rate Na g m⁻² d⁻¹	Rate S g m⁻² d⁻¹	Rate Re g m⁻² d⁻¹
SCT2-2.22	22.05	8.09	70	72	2852	4.7	6.6	539	0.872	9.99E-04	1.59E-03	2.49E-03	7.00E-03	9.09E-03
SCT2-2.23	23.00	8.09	70	73	2746	4.6	6.3	483	0.754	9.82E-04	1.59E-03	2.41E-03	6.23E-03	8.00E-03
Cell SCT2-3														
SCT2-3A	na	nm	80	nm	12	0.42	0.04	105	nm	na	na	na	na	na
SCT2-3B	na	nm	80	nm	10	0.42	0.05	108	0.012	na	na	na	na	na
SCT2-3C	na	nm	80	nm	8.8	0.21	0.04	52	0.012	na	na	na	na	na
SCT2-3.1	1.00	9.44	80	80	5292	5.62	10	134	2.25	2.07E-03	2.00E-03	4.22E-03	8.21E-04	2.63E-02
SCT2-3.2	1.84	9.75	80	85	31379	32	69	449	0.925	1.30E-02	1.28E-02	3.09E-02	6.83E-03	1.14E-02
SCT2-3.3	3.11	8.99	80	84	22659	24	43	270	0.394	9.28E-03	9.48E-03	1.88E-02	3.39E-03	4.71E-03
SCT2-3.6	10.29	9.05	80	83	14724	16	16	124	0.043	5.97E-03	6.25E-03	7.13E-03	6.64E-04	3.75E-04
SCT2-3.11	13.02	9.17	80	36	11398	13	9.6	258	0.491	2.01E-03	2.18E-03	1.83E-03	1.37E-03	2.55E-03
SCT2-3.14	16.07	8.69	80	76	8396	10.0	38	450	1.04	3.12E-03	3.46E-03	1.53E-02	6.15E-03	1.15E-02
SCT2-3.17	19.13	8.77	80	51	16063	17	5.0	1034	2.47	4.01E-03	4.10E-03	1.35E-03	1.08E-02	1.85E-02
SCT2-3.20	20.12	8.92	80	84	13177	14	5.4	1012	2.26	5.39E-03	5.46E-03	2.35E-03	1.73E-02	2.77E-02
SCT2-3.21	21.09	8.79	80	52	13714	15	6.4	1087	2.47	3.48E-03	3.58E-03	1.75E-03	1.16E-02	1.88E-02
SCT2-3.22	22.05	8.85	80	88	10697	12	5.6	895	1.91	4.61E-03	4.77E-03	2.61E-03	1.59E-02	2.46E-02
SCT2-3.23	23.00	8.93	80	61	11876	13	6.9	1043	2.14	3.52E-03	3.58E-03	2.20E-03	1.29E-02	1.90E-02
Cell SCT2-4														
SCT2-4A	na	nm	80	nm	7.8	0.35	0.13	111	0.012	na	na	na	na	na
SCT2-4B	na	nm	80	nm	12	0.43	0.16	98	0.012	na	na	na	na	na
SCT2-4C	na	nm	80	nm	11	0.57	0.20	101	0.012	na	na	na	na	na
SCT2-4.1	1.00	9.87	80	72	26191	29	57	252	0.429	9.24E-03	9.68E-03	2.16E-02	2.39E-03	4.42E-03
SCT2-4.2	1.84	9.46	80	48	27937	30	49	199	0.189	6.58E-03	6.84E-03	1.23E-02	1.03E-03	1.25E-03
SCT2-4.3	3.11	8.92	80	79	21371	24	33	174	0.156	8.34E-03	8.87E-03	1.37E-02	1.25E-03	1.69E-03
SCT2-4.6	10.29	8.97	80	65	15221	17	15.9	126	0.056	4.84E-03	5.24E-03	5.41E-03	3.32E-04	4.17E-04
SCT2-4.11	13.02	9.05	80	38	9929	12	9.5	513	1.15	1.84E-03	2.00E-03	1.86E-03	3.47E-03	6.33E-03
SCT2-4.14	16.07	8.71	80	50	9022	10	35.5	638	1.58	2.22E-03	2.36E-03	9.40E-03	6.02E-03	1.16E-02
SCT2-4.17	19.13	8.69	80	58	16197	18	5.4	1289	2.95	4.60E-03	4.71E-03	1.59E-03	1.54E-02	2.51E-02
SCT2-4.20	20.12	8.87	80	80	12646	14	6.5	1140	2.40	4.95E-03	5.19E-03	2.68E-03	1.85E-02	2.81E-02
SCT2-4.21	21.09	8.79	80	57	13418	15	7.6	1192	2.54	3.73E-03	3.90E-03	2.22E-03	1.38E-02	2.11E-02

Table A1. SPFT pH Sweep Experimental Conditions and Dissolutions Rates

Sample I.D.	Duration day	pH (25°C)	Target Flow rate mL d⁻¹	Actual Flow rate mL d⁻¹	$^aC_{Al}$ µg L⁻¹ [10]^c	C_{Si} mg L⁻¹ [0.10]	C_{Na} mg L⁻¹ [0.10]	C_S µg L⁻¹ [50]	C_{Re} µg L⁻¹ [0.1]	^{b}Rate Al g m⁻² d⁻¹	Rate Si g m⁻² d⁻¹	Rate Na g m⁻² d⁻¹	Rate S g m⁻² d⁻¹	Rate Re g m⁻² d⁻¹
SCT2-4.22	22.05	8.82	80	84	10791	12	6.8	960	1.96	4.45E-03	4.55E-03	2.96E-03	1.62E-02	2.42E-02
SCT2-4.23	23.00	8.91	80	56	10953	12	7.6	1022	2.02	3.03E-03	3.13E-03	2.22E-03	1.16E-02	1.67E-02
Cell SCT2-5														
SCT2-5A	na	nm	90	nm	10	0.2	0.03	106	0.012	na	na	na	na	na
SCT2-5B	na	nm	90	nm	8.5	0.2	0.03	103	0.012	na	na	na	na	na
SCT2-5C	na	nm	90	nm	8.1	0.2	0.04	141	0.012	na	na	na	na	na
SCT2-5.1	1.00	9.76	90	19	32814	34	74	681	1.35	3.10E-03	3.06E-03	7.57E-03	2.43E-03	3.80E-03
SCT2-5.2	1.84	9.56	90	101	26764	28	56	321	0.641	1.32E-02	1.34E-02	2.99E-02	4.62E-03	9.34E-03
SCT2-5.3	3.11	8.89	90	91	18507	20	31	169	0.216	8.23E-03	8.73E-03	1.50E-02	1.06E-03	2.73E-03
SCT2-5.6	10.29	9.43	90	86	16017	18	20	131	0.095	6.72E-03	7.41E-03	8.85E-03	2.82E-04	1.05E-03
SCT2-5.11	13.02	9.49	90	105	13156	15	14	791	1.57	6.73E-03	7.36E-03	7.59E-03	1.58E-02	2.40E-02
SCT2-5.14	16.07	9.79	90	89	15561	17	15	1384	2.46	6.77E-03	7.14E-03	6.81E-03	2.52E-02	3.20E-02
SCT2-5.17	19.13	9.58	90	63	14581	16	13	1466	2.61	4.52E-03	4.76E-03	4.30E-03	1.91E-02	2.42E-02
SCT2-5.20	20.12	9.59	90	93	11424	12	9.7	1035	1.92	5.19E-03	5.37E-03	4.74E-03	1.91E-02	2.61E-02
SCT2-5.21	21.09	9.30	90	66	12645	14	11	1065	1.99	4.07E-03	4.19E-03	3.65E-03	1.40E-02	1.92E-02
SCT2-5.22	22.05	9.49	90	101	10177	11	8.7	784	1.49	5.01E-03	5.27E-03	4.59E-03	1.50E-02	2.19E-02
SCT2-5.23	23.00	9.49	90	76	10814	12	8.8	746	1.40	4.04E-03	4.19E-03	3.52E-03	1.07E-02	1.56E-02
Cell SCT2-6														
SCT2-6A	na	nm	100	nm	18	0.84	0.11	28	nm	na	na	na	na	na
SCT2-6B	na	nm	100	nm	17	0.85	0.13	32	0.012	na	na	na	na	na
SCT2-6C	na	nm	100	nm	24	0.89	0.15	29	0.012	na	na	na	na	na
SCT2-6.1	1.00	nm	100	72	35927	32	132	620	1.66	1.26E-02	1.07E-02	5.02E-02	9.49E-03	1.74E-02
SCT2-6.2	1.84	nm	100	79	39540	38	78	225	0.421	1.53E-02	1.39E-02	3.25E-02	3.45E-03	4.75E-03
SCT2-6.3	3.11	nm	100	92	28972	28	45	183	0.328	1.31E-02	1.21E-02	2.20E-02	3.18E-03	4.30E-03
SCT2-6.6	10.29	11.06	100	96	24961	28	21	465	0.674	1.18E-02	1.22E-02	1.08E-02	9.39E-03	9.40E-03
SCT2-6.11	13.02	11.16	100	117	22427	24	18	143	0.213	1.29E-02	1.30E-02	1.12E-02	2.96E-03	3.47E-03
SCT2-6.14	16.07	11.04	100	99	23845	26	21	128	0.266	1.16E-02	1.17E-02	1.10E-02	2.20E-03	3.73E-03
SCT2-6.17	19.13	10.84	100	81	22771	24	19	173	0.281	9.08E-03	9.04E-03	8.21E-03	2.62E-03	3.23E-03
SCT2-6.20	20.12	10.97	100	106	20139	21	17	232	0.400	1.05E-02	1.04E-02	9.70E-03	4.80E-03	6.06E-03
SCT2-6.21	21.09	10.94	100	70	20657	22	18	214	0.374	7.12E-03	7.13E-03	6.54E-03	2.90E-03	3.75E-03

Table A1. SPFT pH Sweep Experimental Conditions and Dissolutions Rates

Sample I.D.	Duration day	pH (25°C)	Target Flow rate mL d⁻¹	Actual Flow rate mL d⁻¹	[a]C_{Al} µg L⁻¹ [10][c]	C_{Si} mg L⁻¹ [0.10]	C_{Na} mg L⁻¹ [0.10]	C_{S} µg L⁻¹ [50]	C_{Re} µg L⁻¹ [0.1]	[b]Rate Al g m⁻² d⁻¹	Rate Si g m⁻² d⁻¹	Rate Na g m⁻² d⁻¹	Rate S g m⁻² d⁻¹	Rate Re g m⁻² d⁻¹
SCT2-6.22	22.05	10.95	100	107	17640	19	15	281	0.504	9.29E-03	9.41E-03	8.52E-03	6.06E-03	7.80E-03
SCT2-6.23	23.00	10.97	100	82	18879	20	16	331	0.651	7.59E-03	7.49E-03	6.78E-03	5.55E-03	7.73E-03

[a]C_i = average net concentration (effluent-influent) of the element, i.
[b]Rates are calculated using the surface area of 2.37 m²g⁻¹ determined by BET measurement. The mass of sample powders was held constant at 0.5 g.
[c]Limit of quantification determined by the lowest certified standard reading within 10% of true value.
na = not applicable; nm = not measured

Table A2. SPFT Flow Rate Sweep Experimental Conditions and Dissolutions Rates

Sample I.D.	Duration day	pH (25°C)	Target Flow rate mL d^{-1}	Actual Flow rate mL d^{-1}	[a]C_{Al} µg L^{-1} [10]^c	C_{Si} mg L^{-1} [0.20]	C_{Na} mg L^{-1} [0.40]	[d]C_S µg L^{-1} [50]	C_{Re} µg L^{-1} [0.04]	[b]Rate Al g m^{-2} d^{-1}	Rate Si g m^{-2} d^{-1}	Rate Na g m^{-2} d^{-1}	Rate S g m^{-2} d^{-1}	Rate Re g m^{-2} d^{-1}
Cell SCT2-13														
SCT2-13A	na	nm	20	nm	100	0.200	0.400	50	0.040	na	na	na	na	na
SCT2-13B	na	nm	20	nm	100	0.200	0.400	50	0.040	na	na	na	na	na
SCT2-13C	na	nm	20	nm	100	0.200	0.400	50	0.040	na	na	na	na	na
SCT2-13.2	2.10	nm	20	19.1	27250	28.5	111.4	850	1.737	2.6E-03	2.6E-03	1.1E-02	2.9E-03	4.8E-03
SCT2-13.10	10.10	nm	20	10.9	29340	32.6	49.9	583	0.199	1.6E-03	1.7E-03	2.9E-03	2.0E-03	2.6E-04
SCT2-13.18	18.01	8.86	20	16.3	24070	27.3	28.5	521	0.113	1.9E-03	2.1E-03	2.5E-03	2.6E-03	1.8E-04
SCT2-13.22	23.23	8.52	20	18.1	20850	23.5	19.8	234	1.358	1.9E-03	2.0E-03	1.9E-03	7.8E-04	3.6E-03
SCT2-13.26	26.95	8.99	20	24.4	17520	20.1	19.8	129	2.858	2.1E-03	2.3E-03	2.5E-03	3.6E-04	1.0E-02
SCT2-13.34	41.83	8.73	20	18.5	15200	17.8	15.5	60	2.919	1.4E-03	1.6E-03	1.5E-03	5.2E-05	7.9E-03
SCT2-13.36	46.08	8.81	20	16.4	13520	15.4	15.6	162	2.897	1.1E-03	1.2E-03	1.3E-03	4.4E-04	7.0E-03
SCT2-13.38	51.98	8.69	20	18.0	11820	13.7	13.8	928	2.768	1.0E-03	1.2E-03	1.3E-03	5.0E-03	7.3E-03
SCT2-13.39	55.11	8.63	20	18.6	10190	12.2	13.0	1222	2.581	9.3E-04	1.1E-03	1.3E-03	4.7E-03	7.1E-03
SCT2-13.40	56.06	8.61	20	17.9	10670	12.7	13.5	1430	2.773	9.4E-04	1.1E-03	1.3E-03	7.0E-03	7.3E-03
CellSCT2-14														
SCT2-14A	na	nm	40	nm	100	0.2	0.4	nm	0.040	na	na	na	na	na
SCT2-14B	na	nm	40	nm	100	0.2	0.4	nm	0.040	na	na	na	na	na
SCT2-14C	na	nm	40	nm	100	0.2	0.4	nm	0.040	na	na	na	na	na
SCT2-14.2	2.10	nm	40	33.9	27310	28.4	104	nm	1.727	4.6E-03	4.6E-03	1.9E-02	nm	8.5E-03
SCT2-14.10	10.10	nm	40	47.7	19250	21.4	26.5	nm	0.088	4.5E-03	4.9E-03	6.6E-03	nm	3.4E-04
SCT2-14.18	18.01	8.95	40	37.4	13720	15.6	13.3	nm	1.715	2.5E-03	2.8E-03	2.6E-03	nm	9.3E-03
SCT2-14.22	23.23	8.69	40	42.9	12170	13.8	13.3	nm	2.290	2.6E-03	2.8E-03	2.9E-03	nm	1.4E-02
SCT2-14.26	26.95	9.14	40	57.0	10580	12.7	12.4	nm	2.434	3.0E-03	3.4E-03	3.6E-03	nm	2.0E-02
SCT2-14.30	32.99	8.76	40	44.6	9811	11.6	12.3	nm	2.411	2.1E-03	2.4E-03	2.8E-03	nm	1.6E-02
SCT2-14.34	41.83	8.78	40	16.4	8108	9.61	10.4	nm	1.716	6.5E-04	7.4E-04	8.8E-04	nm	4.1E-03
SCT2-14.35	44.11	8.70	40	40.5	7962	9.15	10.1	nm	1.554	1.6E-03	1.7E-03	2.1E-03	nm	9.1E-03
SCT2-14.36	46.08	8.83	40	38.0	7542	8.56	10.2	nm	1.455	1.4E-03	1.5E-03	2.0E-03	nm	8.0E-03
SCT2-14.37	48.85	8.62	40	43.2	7243	8.60	9.52	nm	1.168	1.5E-03	1.7E-03	2.1E-03	nm	7.3E-03
CellSCT2-15														
SCT2-15A	na	nm	60	nm	100	0.2	0.4	nm	0.040	na	na	na	na	na

A.5

Table A2. SPFT Flow Rate Sweep Experimental Conditions and Dissolutions Rates

Sample I.D.	Duration day	pH (25°C)	Target Flow rate mL d^{-1}	Actual Flow rate mL d^{-1}	$^{a}C_{Al}$ μg L^{-1} [10]^{c}	C_{Si} mg L^{-1} [0.20]	C_{Na} mg L^{-1} [0.40]	$^{d}C_{S}$ μg L^{-1} [50]	C_{Re} μg L^{-1} [0.04]	^{b}Rate Al g m^{-2} d^{-1}	Rate Si g m^{-2} d^{-1}	Rate Na g m^{-2} d^{-1}	Rate S g m^{-2} d^{-1}	Rate Re g m^{-2} d^{-1}
SCT2-15B	na	nm	60	nm	100	0.2	0.4	nm	0.040	na	na	na	na	na
SCT2-15C	na	nm	60	nm	100	0.2	0.4	nm	0.040	na	na	na	na	na
SCT2-15.2	2.10	nm	60	58.9	28890	29.2	104.0	nm	1.839	8.3E-03	8.1E-03	3.2E-02	nm	1.6E-02
SCT2-15.10	10.10	nm	60	73.9	11400	13.5	14.0	nm	1.420	4.1E-03	4.7E-03	5.3E-03	nm	1.5E-02
SCT2-15.18	18.01	8.63	60	54.8	9511	10.8	11.8	nm	2.025	2.5E-03	2.8E-03	3.3E-03	nm	1.6E-02
SCT2-15.22	23.23	8.49	60	59.2	8452	9.91	10.7	nm	1.674	2.4E-03	2.7E-03	3.2E-03	nm	1.4E-02
SCT2-15.26	26.95	9.22	60	68.5	7954	9.80	7.56	nm	1.256	2.6E-03	3.1E-03	2.6E-03	nm	1.2E-02
SCT2-15.28	28.78	9.06	60	50.5	8220	9.57	8.51	nm	1.250	2.0E-03	2.3E-03	2.2E-03	nm	9.0E-03
SCT2-15.29	30.99	8.90	60	59.1	7465	8.97	8.29	nm	1.165	2.1E-03	2.5E-03	2.5E-03	nm	9.8E-03
SCT2-15.30	32.99	8.90	60	65.0	7276	8.61	7.62	nm	0.950	2.3E-03	2.6E-03	2.5E-03	nm	8.7E-03
SCT2-15.31	34.92	8.75	60	61.1	6910	8.28	7.81	nm	0.806	2.0E-03	2.4E-03	2.4E-03	nm	6.9E-03
SCT2-15.32	37.89	8.66	60	60.6	6634	8.06	7.52	nm	0.648	2.0E-03	2.3E-03	2.3E-03	nm	5.5E-03
CellSCT2-16														
SCT2-16A	na	nm	80	nm	100	0.2	0.4	nm	0.040	na	na	na	na	na
SCT2-16B	na	nm	80	nm	100	0.2	0.4	nm	0.040	na	na	na	na	na
SCT2-16C	na	nm	80	nm	100	0.2	0.4	nm	0.040	na	na	na	na	na
SCT2-16.2	2.10	nm	80	74.1	23200	23.6	87.6	nm	1.257	8.4E-03	8.3E-03	3.4E-02	nm	1.3E-02
SCT2-16.6	5.99	9.02	80	78.5	15390	17.6	20.2	nm	0.167	5.9E-03	6.5E-03	8.3E-03	nm	1.5E-03
SCT2-16.10	10.10	nm	80	82.8	9799	11.2	10.8	nm	1.302	4.0E-03	4.3E-03	4.6E-03	nm	1.5E-02
SCT2-16.14	13.91	9.41	80	80.6	9466	10.9	10.9	nm	1.590	3.7E-03	4.1E-03	4.5E-03	nm	1.8E-02
SCT2-16.18	18.01	8.76	80	87.8	7252	9.36	11.3	nm	1.574	3.1E-03	3.8E-03	5.1E-03	nm	2.0E-02
SCT2-16.22	23.23	8.48	80	74.7	7840	9.17	9.38	nm	1.217	2.8E-03	3.2E-03	3.6E-03	nm	1.3E-02
SCT2-16.26	26.95	8.76	80	53.2	7432	8.52	8.49	nm	1.006	1.9E-03	2.1E-03	2.3E-03	nm	7.6E-03
SCT2-16.27	27.87	8.58	80	48.0	8152	9.42	9.81	nm	1.040	1.9E-03	2.1E-03	2.4E-03	nm	7.1E-03
SCT2-16.28	28.78	8.74	80	71.3	7915	9.14	9.12	nm	0.935	2.7E-03	3.0E-03	3.3E-03	nm	9.4E-03
SCT2-16.29	30.99	8.75	80	77.6	7689	9.02	8.20	nm	0.724	2.9E-03	3.3E-03	3.2E-03	nm	7.9E-03
CellSCT2-17														
SCT2-17A	na	nm	100	nm	100	0.2	0.4	nm	0.040	na	na	na	na	na
SCT2-17B	na	nm	100	nm	100	0.2	0.4	nm	0.040	na	na	na	na	na
SCT2-17C	na	nm	100	nm	100	0.2	0.4	nm	0.040	na	na	na	na	na

Sample I.D.	Duration day	pH (25°C)	Target Flow rate mL d^{-1}	Actual Flow rate mL d^{-1}	[a]C_{Al} µg L^{-1} [10][c]	C_{Si} mg L^{-1} [0.20]	C_{Na} mg L^{-1} [0.40]	[d]C_S µg L^{-1} [50]	C_{Re} µg L^{-1} [0.04]	[b]Rate Al g m^{-2} d^{-1}	Rate Si g m^{-2} d^{-1}	Rate Na g m^{-2} d^{-1}	Rate S g m^{-2} d^{-1}	Rate Re g m^{-2} d^{-1}
SCT2-17.2	2.10	nm	100	109.9	21620	23.1	68.8	nm	1.073	1.2E-02	1.2E-02	4.0E-02	nm	1.7E-02
SCT2-17.6	5.99	8.99	100	106.6	12760	15.0	16.7	nm	0.253	6.6E-03	7.5E-03	9.2E-03	nm	3.3E-03
SCT2-17.10	10.10	nm	100	96.4	9249	10.5	10.8	nm	1.464	4.3E-03	4.7E-03	5.3E-03	nm	2.0E-02
SCT2-17.14	13.91	9.276	100	95.6	8309	9.32	10.1	nm	1.444	3.8E-03	4.1E-03	4.9E-03	nm	2.0E-02
SCT2-17.18	18.01	8.63	100	98.3	7485	8.79	9.43	nm	1.207	3.6E-03	4.0E-03	4.7E-03	nm	1.7E-02
SCT2-17.22	23.23	8.51	100	99.6	7082	8.13	8.32	nm	0.903	3.4E-03	3.7E-03	4.2E-03	nm	1.3E-02
SCT2-17.26	26.95	8.97	100	103.4	6890	7.96	7.46	nm	0.649	3.4E-03	3.8E-03	3.9E-03	nm	9.3E-03
SCT2-17.27	27.87	8.77	100	103.4	6847	7.98	7.43	nm	0.586	3.4E-03	3.8E-03	3.8E-03	nm	8.3E-03
SCT2-17.28	28.78	8.91	100	98.0	6602	7.94	7.15	nm	0.504	3.1E-03	3.6E-03	3.5E-03	nm	6.7E-03
SCT2-17.29	30.99	8.78	100	98.9	6367	7.62	6.84	nm	0.407	3.0E-03	3.5E-03	3.4E-03	nm	5.3E-03
CellSCT2-18														
SCT2-18A	na	nm	150	nm	100	0.2	0.4	nm	0.040	na	na	na	na	na
SCT2-18B	na	nm	150	nm	100	0.2	0.4	nm	0.040	na	na	na	na	na
SCT2-18C	na	nm	150	nm	100	0.2	0.4	nm	0.040	na	na	na	na	na
SCT2-18.2	2.10	nm	150	154.9	20270	21.8	60.4	nm	0.833	1.5E-02	1.6E-02	4.9E-02	nm	1.8E-02
SCT2-18.4	4.07	8.81	150	142.6	14470	16.8	24.4	nm	0.446	1.0E-02	1.1E-02	1.8E-02	nm	8.5E-03
SCT2-18.6	5.99	8.92	150	167.9	11560	13.8	13.4	nm	0.295	9.5E-03	1.1E-02	1.2E-02	nm	6.3E-03
SCT2-18.7	6.93	8.96	150	143.7	9241	11.1	10.0	nm	0.468	6.5E-03	7.5E-03	7.3E-03	nm	9.1E-03
SCT2-18.8	7.86	8.92	150	147.2	8961	10.5	9.41	nm	0.782	6.4E-03	7.2E-03	7.0E-03	nm	1.6E-02
SCT2-18.9	9.20	nm	150	152.1	8351	9.78	8.79	nm	0.983	6.2E-03	6.9E-03	6.8E-03	nm	2.1E-02
CellSCT2-19														
SCT2-19A	na	nm	200	nm	100	0.2	0.4	nm	0.040	na	na	na	na	na
SCT2-19B	na	nm	200	nm	100	0.2	0.4	nm	0.040	na	na	na	na	na
SCT2-19C	na	nm	200	nm	100	0.2	0.4	nm	0.040	na	na	na	na	na
SCT2-19.2	2.10	nm	200	209.8	17870	19.2	44.3	nm	0.703	1.8E-02	1.9E-02	4.9E-02	nm	2.1E-02
SCT2-19.4	4.07	8.70	200	207.1	9473	10.1	12.7	nm	0.066	9.6E-03	9.8E-03	1.4E-02	nm	7.9E-04
SCT2-19.6	5.99	8.86	200	202.9	7501	8.41	7.26	nm	0.403	7.4E-03	8.0E-03	7.4E-03	nm	1.1E-02
SCT2-19.7	6.93	8.94	200	192.6	5612	6.56	5.82	nm	0.571	5.2E-03	5.9E-03	5.6E-03	nm	1.5E-02
SCT2-19.8	7.86	8.90	200	200.9	5544	6.36	5.88	nm	0.792	5.4E-03	5.9E-03	5.9E-03	nm	2.2E-02
SCT2-19.9	9.20	nm	200	196.7	5460	6.05	5.57	nm	0.775	5.2E-03	5.5E-03	5.4E-03	nm	2.1E-02

[a]C_i = average net concentration (effluent-influent) of the element, i.
[b]Rates are calculated using the surface area of 2.37 m^2g^{-1} determined by BET measurement. The mass of sample powders was held constant at 0.5 g.
[c]Limit of quantification determined by the lowest certified standard reading within 10% of true value.
[d]Sulfur concentrations were determined on samples collected at sampling times adjacent to the times listed. Analytical problems prevented obtaining sulfur concentrations on all samples.
na = not applicable; nm = not measured

APPENDIX B – PUF TEST DATA

Table B1. Effluent Chemical Analyses (mg L^{-1}) and Average Water Content in PUF02A Test[1]

Sample ID	Time, h	θ	σ_θ	Al	Na	Si	S	Re
SRA-1	1.9	0.455	0.185	43.31	4,011	120.4	93.71	0.104
SRA-2	2.8	0.295	0.052	209.4	2,788	89.72	57.92	0.062
SRA-3	13.9	0.212	0.014	519.3	3,776	74.92	59.48	0.059
SRA-4	38.3	0.233	0.012	789.8	6,085	85.71	87.27	0.093
SRA-5	65.7	0.242	0.015	904.4	6,674	124.5	74.11	0.097
SRA-6	88.5	0.284	0.013	841.4	6,418	147.8	48.56	0.080
SRA-7	111.9	0.337	0.018	845.3	6,071	178.9	24.17	0.071
SRA-8	133.4	0.383	0.009	663.9	6,513	171.7	8.864	0.068
SRA-9	198.1	0.383	0.009	369.2	5,700	186.0	5.108	0.051
SRA-10	198.6	0.541	0.094	155.5	1,819	81.10	7.064	0.017
SRA-11	232.9	0.373	0.048	231.1	1,600	109.8	4.805	0.018
SRA-12	276.6	0.377	0.018	262.0	1,762	114.4	3.572	0.019
SRA-13	309.2	0.397	0.027	272.3	1,760	103.8	2.706	0.015
SRA-14	355.8	0.407	0.023	267.5	1,593	95.80	2.499	0.011
SRA-15	415.1	0.398	0.021	262.7	1,466	92.94	3.454	0.011
SRA-16	476.9	0.410	0.022	239.5	1,298	88.27	2.498	0.010
SRA-17	559.9	0.410	0.020	250.9	1,272	90.61	3.906	0.010
SRA-18	640.7	0.409	0.023	214.2	1,017	83.40	4.499	0.008
SRA-19	691.2	0.412	0.026	8.403	904.4	1.937	4.340	0.007
SRA-20	799.3	0.414	0.025	32.83	735.8	1.102	4.600	0.006
SRA-21	978.1	0.411	0.035	194.0	640.4	64.90	7.070	0.008
SRA-22	1171.4	0.394	0.028	182.2	569.1	63.28	8.260	0.009
SRA-23	1386.3	0.387	0.031	6.396	609.7	1.485	8.200	0.013
SRA-24	1589.4	0.379	0.023	31.84	432.8	1.945	7.530	0.012
SRA-25	1760.9	0.376	0.024	149.1	405.6	55.39	12.60	0.013
SRA-26	1933.4	0.380	0.020	137.3	365.2	50.61	12.50	0.012
SRA-27	2102.7	0.383	0.026	124.4	366.8	47.64	14.70	0.014
SRA-28	2220.6	0.375	0.022	5.336	337.8	1.550	7.810	0.013

[1]Test conditions were as follows:
total porosity = 0.655
volumetric flow rate = 2 mL/d
temperature = 99°C
column diameter = 0.0191 m
column length = 0.0762 m
specific surface area of FBSR product = 0.183 m^2/g
bulk density of FBSR product = 2.76 g/cm^3

Table B2. Effluent Chemical Analyses (mg L^{-1}) and Average Water Content in PUF02B Test[1]

Sample ID	Time, h	θ	σ_θ	Al	Na	Si	S	Re
SRB-1	2.0	0.388	0.180	24.51	2,640	52.62	65.52	0.056
SRB-2	2.7	0.058	0.000	309.0	4,010	55.26	90.80	0.082
SRB-3	16.5	0.085	0.038	479.4	3,478	113.5	108.3	0.039
SRB-4	43.6	0.180	0.044	505.3	6,039	199.9	177.3	0.057
SRB-5	66.3	0.257	0.012	606.6	10,009	352.5	172.0	0.094
SRB-6	97.1	0.321	0.026	372.4	7,680	226.8	183.7	0.073
SRB-7	145.1	0.480	0.073	18.76	116.3	27.93	2.833	0.003
SRB-8	178.9	0.340	0.061	0.342	56.87	14.37	4.468	0.007
SRB-9	222.5	0.339	0.006	30.65	59.93	31.90	3.503	0.003
SRB-10	255.2	0.349	0.005	0.119	65.67	11.81	3.838	0.003
SRB-11	301.8	0.338	0.008	0.072	32.95	10.70	2.951	0.002
SRB-12	361.0	0.341	0.006	0.639	40.93	12.20	5.411	0.004
SRB-13	422.8	0.344	0.004	0.217	26.66	9.307	3.371	0.003
SRB-14	505.8	0.361	0.013	63.16	172.0	46.08	9.838	0.011
SRB-15	586.6	0.386	0.006	78.44	223.9	46.51	5.692	0.008
SRB-16	637.1	0.399	0.005	31.26	257.6	18.05	8.200	0.007
SRB-17	745.2	0.432	0.029	5.956	272.4	4.586	4.390	0.007
SRB-18	924.1	0.486	0.038	6.227	254.0	4.297	4.860	0.009
SRB-19	1117.3	0.290	0.220	25.71	257.9	6.040	12.90	0.008
SRB-20	1332.2	0.244	0.115	1.789	256.0	6.792	12.00	0.010
SRB-21	1538.9	0.487	0.053	17.42	246.9	9.310	10.00	0.006
SRB-22	1710.5	0.210	0.010	15.98	115.7	16.34	9.790	0.004
SRB-23	1879.5	0.228	0.006	10.99	151.8	9.044	10.10	0.013
SRB-24	2048.8	0.239	0.010	3.310	231.1	4.164	9.950	0.014
SRB-25	2166.6	0.288	0.025	93.99	318.4	42.67	18.60	0.021

[1]Test conditions were as follows:
total porosity = 0.655
volumetric flow rate = 2 mL/d
temperature = 99°C
column diameter = 0.0191 m
column length = 0.0762 m
specific surface area of FBSR product = 0.183 m^2/g
bulk density of FBSR product = 2.76 g/cm^3

DISTRIBUTION

No. of Copies		No. of Copies	
OFFSITE		**ONSITE**	

No. of Copies			
1	Westinghouse Savannah River Company	22	Battelle - Pacific Northwest Division

OFFSITE

1   <u>Westinghouse Savannah River Company</u>
    C. M. Jantzen
    P. O. Box 616
    Aiken, SC 29802

ONSITE

22 <u>Battelle - Pacific Northwest Division</u>

D. H. Bacon	K9-33
T. M. Brouns (5)	K9-69
D. E. Kurath	P7-28
P. F. Martin	K6-81
D. E. McCready	K8-93
B. P. McGrail (5)	K6-81
R. D. Orr	K6-81
A. N. Primak	K8-98
E. A. Rodriguez	K6-81
H. T. Schaef	K6-81
Project File (2)	P7-28
Information Release (2)	K1-06

8   <u>Bechtel National, Inc.</u>

K. H. Abel	H4-02
A. V. Arakali	H4-02
S. M. Barnes	H4-02
W. L. Graves	H4-02
H. R. Hazen	H4-02
G. L. Smith	H4-02
W. L. Tamosaitis	H4-02
WTP PDC Coordinator	H4-02

4   <u>CH2M Hill Hanford, Inc.</u>

M. E. Johnson	L4-07
D. W. Hamilton	H6-03
F. M. Mann	E6-35
R. E. Raymond	H6-22

3   <u>U.S. Department of Energy Richland Operations Office</u>

C. A. Babel	H6-60
P. E. Lamont	H6-60
J. E. Orchard	H6-60